Kinematics and Dynamics of an In-Parallel-Actuated Soft Robot Manipulator

Olalekan Ogunmolu

***Abstract*—A completely soft parallel multi-degree of freedom robot is here put forward to counterbalance the heretofore preoccupation with in-parallel rigid robot mechanisms, typically prevalent in frameless and maskless cranial radiation therapy for 6-DOF real-time patient motion correction. Steel-cast or resin-like assembly robot links have their disadvantages particularly in the error magnification at the tool frame owing to the flexure of torques at previous joints, and their uneven load-to-weight ratios. We study the kinematics of our entirely soft robot mechanism using continuum mechanics and differential geometry. We then derive the Newton-Euler system of equations using elasticity theory. Relating the solutions to the boundary value problem of the Cauchy stress for the soft robots links to the force wrenches on the object/load, we write out the manipulation map and construct the associated Jacobian for its direct positioning analysis. Within the isochoric and contrained shear deformation bounds here set, the mechanism is principally intended to provide a minimally-invasive patient motion correction in lieu of the rigid frames and masks in radiation therapy clinics today. Our goal is to edge open the door a little further towards in-parallel soft actuation mechanisms that do not attenuate the radiation beam, are minimally-invasive, and are comfortable for the patient whilst preserving radiation dose efficacy and treatment efficiency. This is a work in progress and suggestions are welcome.**

I. INTRODUCTION

This work is principally a continuation of the model verified in [1]. Here, we present the systematic analysis of the in-parallel-actuated mechanism. A major application possibility is the real-time closed-loop automatic motion deviation correction, particularly during beam-on time, in robotic radiosurgery; this is a desperately needed technology that has the potential benefits of hastening the current treatment time in clinics, minimizing patient discomfort post-treatment (as opposed to rigid frames and masks currently used in frame and mask-based RT), as well as drastically improving the dose efficacy so that the patient's treatment can be effectively fractionated [2]. It could also find applications in the animation industry where animated plushes are required to be accurately actuated to specific configurations [3], [4]. The real-time control of hyperelastic materials is another possible application [5], [6].

In 2019, an estimated 1,762,450 new cases of cancer will be diagnosed in the United States and 606,880 people will die from the disease. The burden of cancer care is financially significant with estimated national expenditures $147.3 billion in 2017 [7]. Along with surgery and chemotherapy, radiation therapy (RT) is an essential part of a successful cancer treatment, with more than 50% of all patients receiving RT for the management of their cancers. There have been steady gains in the five-year survival rate for cancer patients, with an improvement of 66% across all cancer types. The increase in survival rate has been attributed in a large part to technological advancements in RT. RT can now tightly conform the radiation dose to the 3D shape of a tumor with approximately 1-2 mm accuracy. This allows for further dose escalation to the tumor, while minimizing dose to nearby healthy organs-at-risk (OAR), and has had significant impact on cancer patients in terms of better tumor control and normal tissue sparing. Unfortunately, RT is currently considered as a static process, whereby treatment plans are calculated based on a snapshot (initial CT scan) of the patient anatomy prior to treatment, and then delivered over the course of a number of weeks. This assumption, that the patients internal anatomy maintains the same position as in the initial CT snapshot over the entire course of treatment is incorrect, and is not compatible with modern RT technology, which can now target radiation dose to the tumor at the millimeter level. Issues involving internal anatomic motion during treatment have become ever more critical to address, and currently limit the potential of modern RT. As an example, for prostate cancer, even with the correct initial patient setup at the linear accelerator (LINAC), the prostate can undergo a wide variety of motions once RT has started, with sudden excursions beyond target in excess of 10mm taking place within a few seconds. As the prostate is located directly between the bladder and rectum, such motion can lead to incomplete prostate irradiation and unwanted irradiation of the bladder, urethra, rectum, erectile tissues, or sphincters resulting in serious health issues such as incontinence, rectal leakage, or other tissue toxicity [8].

We call the individual soft robots in our mechanism inflatable air bladders (IABs) owing to their hollow internal chambers that admit or release air based on an applied internal pressurization. We make the fundamental assumption that the IAB's deformation follows the isochoric deformation principle, with reasonable local volume preservation during deformation constraints baked into the physical IAB material properties. We derive the manipulator map, kinematics, Jacobian and end-effector velocities. Soft robots are notoriously difficult to control, given their continuum-based mechanical properties, and the inter-dependency of the parameters that characterize their deformation. It is not surprising that different schemes for controlling soft continuum robots have appeared in literature with mixed successes [9]–[15]. For an extensive

Perelman School of Medicine, The University of Pennsylvania, Philadelphia, PA 19104, USA. Olalekan.Ogunmolu@pennmedicine.upenn.edu

The research reported herein was supported by National Cancer Institute of the National Institutes of Health under award number R01CA227124.

TABLE I
COMMON NOTATIONS IN ARTICLE

Notation	Definition
B	A set of points or particles on IAB Body, B
$\mathscr{B}_\circ$	Closure of the open set of points B in in the reference configuration (arbitrarily chosen) $\boldsymbol{\chi}_0$ over which a non-negative measure of mass is defined.
$\boldsymbol{\chi}(X)$	The motion $\boldsymbol{\chi}$ of particles X in $\mathscr{B}$, viz., a one-to-one mapping, from particles, X, of B to their regions in the 3-dimensional Euclidean space $\mathcal{E}$, such that $\boldsymbol{\chi} : B \to \mathcal{E}$ The *place* of particle X in configuration $\boldsymbol{\chi}$ is $\boldsymbol{X}$[1].
$X = \boldsymbol{\chi}^{-1}(\mathbf{x})$	A region occupied by $\mathbf{x}$ (the Euclidean equivalent of $\boldsymbol{X}$) in configuration $\boldsymbol{\chi}$. Essentially, the inverse of the motion $\boldsymbol{\chi}(\cdot)$. [2]
$\mathbf{F}$	The deformation gradient tensor, $\mathbf{F} = \nabla \boldsymbol{\chi}_k(\boldsymbol{X}) = \dot{\boldsymbol{\chi}}_k(\boldsymbol{X})$.
$\mathbf{C}$	The right Cauchy-Green Tensor, $\mathbf{C} = \mathbf{F}^T\mathbf{F}$.
$\mathbf{B}$	The left Cauchy-Green Tensor, $\mathbf{B} = \mathbf{F}\mathbf{F}^T$.
$\mathbf{v}(\mathbf{x})$	The velocity field $\dot{\boldsymbol{\chi}}(\mathbf{x}) = \dot{\boldsymbol{\chi}}(\boldsymbol{\chi}^{-1}(\boldsymbol{X}))$, where without loss of generality, we have taken $X = \boldsymbol{X}$, *i.e.* the place of X.
$\mathbf{a}(\mathbf{x})$	The acceleration field $\ddot{\boldsymbol{\chi}}(\mathbf{x}) = \dot{\mathbf{v}}(\mathbf{x})$.
$\boldsymbol{\sigma}$	The Cauchy stress tensor.

literature review of the control of continuum soft robots, we refer readers to [16].

The soft robot mechanism consists of IABs connected with extensible couplings (not shown in Figure 3); these couplings are chosen to exploit the soft structures' design for impedance control of the H&N region of the patient. We analyze the manipulation map, the Jacobian of the IAB chains, as well as the contact equations between the IAB mechanism system and patient's cranial region. This paper is a sequel to our previous works [2], [10], [17]–[20]; additionally, we expand upon the kinematics and dynamics of the multi-DOF soft actuation system for H&N motion compensation in RT. Our design goals include a system that (1) provides patient comfort whilst manipulating human body parts necessary for trajectory following during RT, (2) assures dose efficacy while not attenuating the ionizing radiation dose treatment due to undesirable material properties (3) capable of emerging complex

[1]NB: We have dropped the explicit dependence on time due to the final deformation configuration that is of interest to us. Throughout the rest of this paper, we take $\boldsymbol{\chi}$ to be a C^2 diffeomorphism.

[2]Note that $\boldsymbol{\chi}$ and $\boldsymbol{\chi}^{-1}$ are continuous functions of their argument.

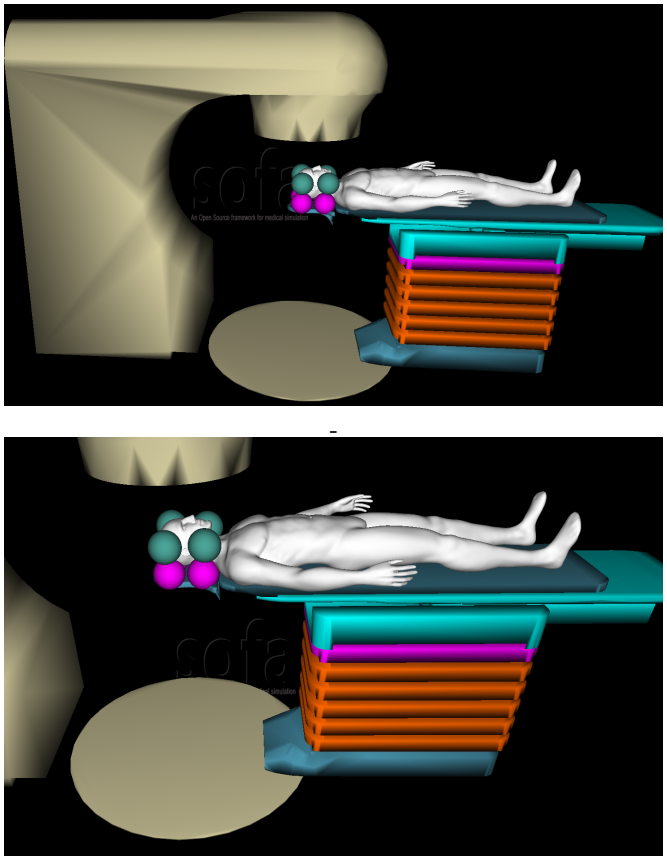

Fig. 1. System setup in the SOFA Framework Architecture. **Top**: Gantry, Turntable, Patient and IAB Chains around the patient's H&N Region. **Bottom**: Close-up view of compensating IABs around patient's H&N region with the patient lying in a supine position on the treatment couch. [Image best visualized in colored ink].

morphological computational behavior with deformable soft robots – simplifying complex patient motion planning and control during robotic RT treatment.

The rest of this paper is organized as follows: in § III, we briefly review the hardware setup and system configuration, we analyze the contact kinematics in § V, describing the contact model, and how we solve the boundary value problem for the IABs' deformation. In § VII, we derive the mechanism's end-effector velocities and forces, and then derive the Newton-Euler Lagrangrian relationship in § VI. We present manipulation examples in the SOFA framework in **??** and conclude the paper in § IX. Proofs and derivations are provided in appendices A, B, and C.

II. MECHANISM DESCRIPTION

In our previous F&M RT IAB control investigation [10], we relied on a system identification approach to realize the overall system model. Our resultant model lumped the patient, treatment couch, as well as IAB models into one. The disadvantage of this approach was that such overall model lacked enough fidelity such that it necessitated the memory-based adaptive control composite laws that was derived from inverse Lyapunov analysis. Furthermore, the approximation model component of the ensuing neural-network controller required extensive training to realize a suitable controller for our H&N

immobilization. Our goal here is to realize constitutive models for the IAB chains – capable of manipulating the patient's H&N's complete DOF motion in real-time during RT. This would enable us to write closed-form expressions for the IAB chains' complete kinematics.

III. Mechanism Description

In our previous F&M RT IAB control investigation [10], we relied on a system identification approach to realize the overall system model. Our resultant model lumped the patient, treatment couch, as well as IAB models into one. The disadvantage of this approach was that such overall model lacked enough fidelity such that it necessitated the memory-based adaptive control composite laws that was derived from inverse Lyapunov analysis. Furthermore, the approximation model component of the ensuing neural-network controller required extensive training to realize a suitable controller for our H&N immobilization. Our goal here is to realize constitutive models for the IAB chains – capable of manipulating the patient's H&N's complete DOF motion in real-time during RT. This would enable us to write closed-form expressions for the IAB chains' complete kinematics.

A. Mechanism Setup

We now describe the mechanism of the complete motion compensation system. We propose 3 IAB kinematic chains totaling 4 IABs around the patient's H&N region as illustrated in Figure 3. The half-sphere IABs have an internal cavity surrounded by shells which are made out of incompressible rubber materials. For simulation purposes, the internal shell has a wall thickness of 0.5cm. This internal cavity contributes a degree of freedom to a soft actuator mechanism in the system – in part holding the head in place and moving the head as needed on the treatment table. The outer shell encapsulates the inner shell such that local volume preservation is fulfilled between configuration changes. This isochoric property and the incompressibility constraints of the IAB material is important in the mathematical derivations of the mechanism's constitutive model. Each IAB in the closed kinematic chain is linked to the couch – each supporting only a part of the total load, redistributing link-loads and solving) some of the problems with serial links. uld like to have the contacting regions between the IABs and head and neck locations to have regions of their surfaces shaped into profiles that allow continuous contact along e.g. a curve or a straight line. This would enforce nonholonomic constraints as the bodies roll without slipping at the *region of contact* on one another. This way, the load that an IAB supports would be distributed over a narrow strip, essentially an atlas, rather than a localized region around a point. An engaging pair of 3D-printed teeth on spur gears would touch along a straight line; helical, hypoid or worm gears would have engaging teeth along complicated spatial curves that enforce this constraint. This constraint is important since it would allow us define the profile of the motion when the IAB exerts a motion on the head.

B. Nonholonomic Contact Profile Design

The IABs change their configuration based on air that flows into or out of their air chambers when the sensed deviation of the patient from a target exceeds a pose setpoint or a desired trajectory path. The degrees of freedom of the mechanism can be determined using *Gruëbler-Kutzbach's mobility condition*, wherein the number of degrees of freedom, or for short freedom, of the mechanism is given by

$$F = 3(n - g - 1) + \sum_{i=1}^{g} f_i \tag{1}$$

where n is the number of links in the mechanism, g is the number of joints, f_i is the total number of degrees of freedom for the ith joint given the planar motion associated with the freedoms of the joints. Therefore, we have through (2) that the mechanism has 8 dofs.

C. Finite Elastic Deformation Model

We propose a finite elastic deformation model [21]–[23], based on the deformation invariants of the stored energy function of each IAB. In what follows, we briefly describe our motivation for devising a finite elastic deformation model. The constant curvature approach for parameterizing the deformation of continuum robots [24]–[26] has played a significant role in the kinematic synthesis of deformable continuum models over the past three decades. Under this framework, the configuration space of a SoRo module is parameterized by the curvature of an arc projected on the SoRo's body, the arc's length, and the angle subtended by a tangent along that arc. The relationship between these parameters are typically found using differential kinematics with a Frenet-Serret frame that models a curve on the SoRo's surface with or without torsion.

By abstracting an infinite dimensional structure to 3D, large portions of the manipulator dynamics are discarded under the assumption that the actuator design is symmetric and uniform in shape. This makes the constant curvature model overly simplistic so that it often exhibits poor performance in position control [27]. While the Cosserat brothers' beam theory has been relatively successful in modeling soft continuum dynamics [28], [29], its complexity, and sensing cost does not justify the alternatives [16].

D. Mechanism Setup

We now describe the mechanism of the complete motion compensation system. We propose 3 IAB kinematic chains totaling 8 IABs around the patient's H&N region as illustrated in Figure 3. The IABs have an internal cavity surrounded by two shells, which are made out of incompressible rubber materials with a Poisson's ration of approximately 0.5. For simulation purposes, the internal shell has a wall thickness of 2.5cm.

The internal cavity ensures the hollow IAB holds the head in place. The outer shell encapsulates the inner shell such that local volume preservation is fulfilled between configuration changes. This isochoric property and the incompressibility

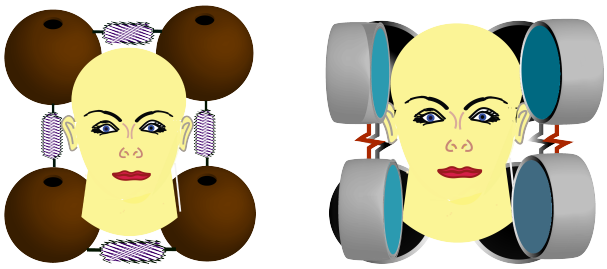

Fig. 2. An abstraction of the patient's position correction mechanism. In the left image, there are four IABs that constitute the base kinematic chain. They lift the head along the Z-axis (up or down on the treatment table) as well as provide pitch motion corrections. On the right, the side kinematic chains provide roll and yaw motion corrections. [Image best visualized in colored print].

constraints of the IAB material is important in the mathematical derivations of the mechanism's constitutive model. Each IAB in the closed kinematic chain is linked to the couch – each supporting only a part of the total load, redistributing link-loads and solving) some of the problems with serial links. uld like to have the contacting regions between the IABs and head and neck locations to have regions of their surfaces shaped into profiles that allow continuous contact along e.g. a curve or a straight line. This would enforce nonholonomic constraints as the bodies roll without slipping at the *region of contact* on one another. This way, the load that an IAB supports would be distributed over a narrow strip, essentially an atlas, rather than a localized region around a point. An engaging pair of 3D-printed teeth on spur gears would touch along a straight line; helical, hypoid or worm gears would have engaging teeth along complicated spatial curves that enforce this constraint. This constraint is important since it would allow us define the profile of the motion when the IAB exerts a motion on the head.

E. Nonholonomic Contact Profile Design

There are two IAB chains to each side of the patient's cranial region, each consisting of two IABs, linked by passive extensible connectors to accommodate head contact throughout manipulation – an important property for our contact kinematics. Each IAB makes contact with the forehead and the chin/neck region at either symmetry of the patient's head. Underneath the patient's H&N regions is a third closed kinematic chain. This chain consists of four IABs, each positioned at four cardinal contact points beneath the patient's H&N region (see Figure 2, and Figure 3). The wearable mask of **??** is configurable to hold the chains in place around the patient's H&N region. The IABs change their configuration based on air that flows into or out of their air chambers when the sensed deviation of the patient from a target exceeds a pose setpoint or a desired trajectory path. The degrees of freedom of the mechanism can be determined using *Gruëbler-Kutzbach's mobility condition*, wherein the number of degrees of freedom of the mechanism is given by (when the actuation results in a

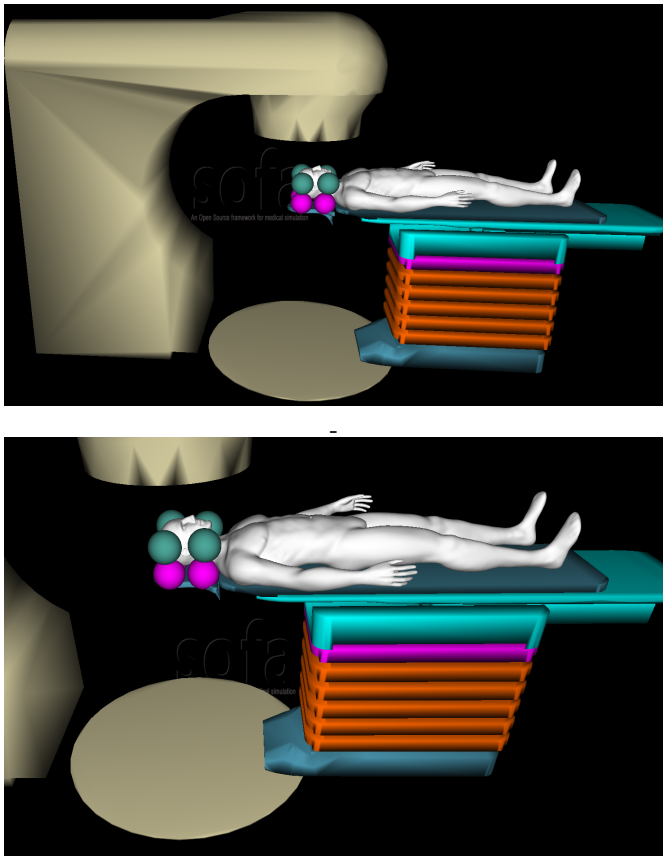

Fig. 3. System setup in the SOFA Framework Architecture. **Top**: Gantry, Turntable, Patient and IAB Chains around the patient's H&N Region. **Bottom**: Close-up view of compensating IABs around patient's H&N region with the patient lying in a supine position on the treatment couch. [Image best visualized in colored print].

non-planar workspace configuration)

$$F = 6(N - g) + \sum_{i=1}^{g} f_i \tag{2}$$

where N is the number of links in the mechanism, g is the number of joints, f_i is the total number of degrees of freedom for the ith joint. where through equations (2), the mechanism of has 16 DOFs given its $N = 8$ links, $g = 8$ joints, and each IAB joint is constrained along 2 DOFs .

IV. Deformation Parameterization in Generalized Coordinates

For a background material on this section, readers are encouraged to read [2, §2-§3] and [22]. The commonly used notations throughout this paper is listed in Table I. At a material point $\mathbf{X}$ of the IAB surface in a configuration $\mathscr{B}_\circ$, it can be verified that the tensor $\mathbf{C} - \mathbf{I}$ represents a change in length of an arbitrary line element of the material, where $\mathbf{C}$ is the right Cauchy-Green Tensor as defined in [1]. For the material to be unstrained, we must have the Lagrangean strain tensor as zero $i.e.$

$$\mathbf{E} = \frac{1}{2}(\mathbf{C} - \mathbf{I}) = 0.$$

A particle $\mathbf{X}$'s displacement from the reference to the current configurations must be such that the point difference $d = \mathbf{x} - \mathbf{X}$

is $d(\mathbf{X}) = \boldsymbol{\chi}(\boldsymbol{X}) - \mathbf{X}$, where $\boldsymbol{\chi}(\boldsymbol{X})$ follows our notation in [1]. We can therefore characterize the point differences by the two-point *displacement gradient*,

$$\mathbf{D} = \text{Grad } d(\mathbf{X}) = \mathbf{F} - \mathbf{I}. \tag{3}$$

If we define unit vectors $\mathbf{m}$ and $\mathbf{M}$ tangent to fibers $\mathbf{dx}$ and $\mathbf{dX}$ in the current and reference configurations respectively, it follows from the invariant of deformation that

$$\mathbf{m}|\mathbf{dx}| = \mathbf{FM}|\mathbf{dX}| \implies |\mathbf{dx}|^2 = \mathbf{M}\cdot(\mathbf{CM})|\mathbf{dX}|^2. \tag{4}$$

Whence, the *stretch* between line elements $\mathbf{dx}$ and $\mathbf{dX}$ is

$$\lambda(\mathbf{M}) = \frac{|\mathbf{dx}|}{|\mathbf{dX}|} = |\mathbf{FM}| \equiv (\mathbf{M}\cdot(\mathbf{CM}))^{\frac{1}{2}}. \tag{5}$$

Lastly, we define two line elements $\mathbf{dX}$ and $\mathbf{dX}'$ with unit tangent vectors $\mathbf{M}$ and $\mathbf{M}'$ at points $\mathbf{X}$ and $\mathbf{X}'$ in the reference configuration; these fibers correspond to $\mathbf{dx}$ and $\mathbf{dx}'$ with unit vectors $\mathbf{m}$ and $\mathbf{m}'$ at points $\mathbf{x}$ and $\mathbf{x}'$ in the current configuration. Let β denote the angle between the directions $\mathbf{M}$ and $\mathbf{M}'$ and let α be the angle between directions $\mathbf{m}$ and $\mathbf{m}'$; then

$$\mathbf{dx} = \mathbf{FdX}, \quad \mathbf{dx}' = \mathbf{FdX}', \quad \beta = \cos^{-1}(\mathbf{M}\cdot\mathbf{M}'), \tag{6a}$$

$$\text{and } \alpha = \cos^{-1}(\mathbf{m}\cdot\mathbf{m}') = \cos^{-1}(\mathbf{M}\cdot(\mathbf{CM}')/\lambda(\mathbf{M})\cdot\lambda(\mathbf{M}')). \tag{6b}$$

In the plane of shear of $\mathbf{M}$ and $\mathbf{M}'$, the *angle of shear* between the material line elements is the reduction in angles

$$\phi = \beta - \alpha. \tag{7}$$

Examining (3), and (5), we notice that they are both characterized by the stretch $\lambda = r/R$ and the radius in the current configuration (c.f. [1]). Therefore, we take the kinematic quantities that characterize the IAB deformation as

Generalized Coordinates

$$\mathbf{r} = \begin{bmatrix}\lambda\\ r\\ \phi\end{bmatrix} = \begin{bmatrix} r/R \\ (R_\circ^3 + r_i^3 - R_i^3)^{1/3} \\ \beta - \alpha\end{bmatrix} \tag{8}$$

i.e. $\mathbf{r}$ is a function of material stretch, the angle of shear between material line elements, and the shell radius, r. Equation (8) denotes the generalized coordinates of an IAB within the mechanism, where $R_\circ$ is the external radius in the reference configuration, and R_i and r_i are respectively the internal radii in the reference and current configurations. This is a reasonable coordinate since the deformation at any region of the IAB material can be characterized by the amount of shear, stretch or radius change [1].

V. Analysis of Contact Kinematics

The manipulators and head are considered as linear elastic object materials with the interaction at the head and an IAB contact considered as a classical case of two elastic bodies in contact. We model the contact type between the head and an IAB similar to the soft finger contact primitive of [30]. Here, our soft contact is the convex sum of *point contacts* with friction over the small area of contact. IAB forces and torques are modeled within a "cone of forces" about the direction of the surface normal from a patient's head (see Figure 4). The trajectory of the head under the influence of motion of an IAB is influenced by the position vector $\mathbf{r}$ described in [1]. When the IAB deforms, body forces over its current configuration and contact (*traction*) forces over its boundary $\partial\mathcal{B}$ impact motion on the head. Constrained by the frictional coefficient, we define the soft contact force inside the friction cone as

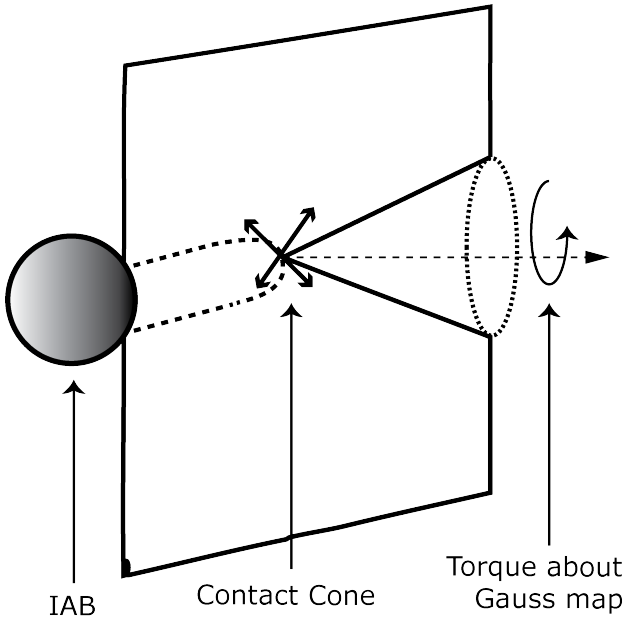

Fig. 4. Illustration of the IAB Soft Contact Type

$$\tilde{F}_{c_i} = \begin{bmatrix}\mathbf{I} & 0\\ 0 & n_{c_i}\end{bmatrix}\begin{bmatrix} f_{c_i}\\ \tau_{c_i}\end{bmatrix}, \tag{9}$$

where $f_{c_i} \in \mathbb{R}^3$ denotes the amount of force exerted by the IAB along the direction of contact, $\tau_{c_i} \in \mathbb{R}$ is the moment of the contact force, and n_{c_i} is the *normal* or *Gauss map*[3] for a manifold $S \subset \mathbb{R}^3$ of a head surface. For contact models with friction, we require that all contact forces lie within the friction cone, determined by the frictional coefficient. The set of forces within or on the boundary of the friction cone is

$$FC = \{f_c \in \mathbb{R}^n : \|f_{c_{ij}}^t\| \le \mu_{ij}\|f_{c_i}^n\|, \\ i = 1,\dots,k,\ j = 1,\dots,m_i\} \tag{10}$$

where $f_{c_{ij}}^t$ is the tangent component of the j^{th} element of the contact force, $f_{c_i}^n$ is i^{th} contact's normal force, and μ_{ij} is $f_{c_{ij}}$'s coefficient of friction.

A. Boundary Value Problem for IAB Deformation

In general, we expect the isochoric deformation principle to hold for the side IAB chains and that our analysis in [1] holds for these actuators. For these actuators, the position vector on the IAB material body is given by (8) with ϕ set to zero. We now solve the boundary-value problem for the IAB

[3]A normal map for a manifold S is a continuous map $g : S \to S^2 \subset \mathbb{R}^3$such that for every $s \in S, g(s)$ is orthogonal to S at s [31].

deformation when the head rests on the base IABs. Again, we assume a spherically-symmetric deformation constraint imposed on the IAB when the head rolls or slips. This may be achieved via an appropriate vulcanization of the IAB rubber material, for example (see [21] or [32]). First, we define mass-density ρ of the IAB material. Suppose α is a location of $\mathscr{B}$. Any massy part $\mathscr{P}$ of $\mathscr{B}$'s mass is the Lesbesgue integral of the non-negative mass-density ρ over the location of $\mathscr{P}$ such that

$$M(\mathscr{P}) = \int_{\alpha(\mathscr{P})} \rho_\alpha dV. \tag{11}$$

For an IAB material in contact with the head, the applied forces on the current configuration of the IAB body $\mathscr{B}$ are

- the body forces, $b(\cdot)$, over volume element dv

$$\int_{\mathscr{B}} \rho(\mathbf{x}, t)\boldsymbol{b}(\mathbf{x}, t)dv; \tag{12}$$

- the contact forces, $f_c(\cdot)$ over a smooth oriented surface in $\mathscr{B}$ including the boundary $\partial\mathscr{B}$ of $\mathscr{B}$,

$$\int_{\partial\mathscr{B}} f_c(\mathbf{x}, \partial\mathscr{B})da, \tag{13}$$

  - we take the contact force to mean the frictional force tangential to the IAB surface as well as surface pressure; and
- the gravitational force of the head mass acting along the direction of contact, f_g.

We make the explicit assumption that mass is an absolutely continuous function of volume and the head maintains contact with the IAB throughout deformation. This is a reasonable assumption given the tight kinematic arrangement around the cranial region as seen in Figure 3. Suppose that for the i^{th} IAB in the chain, r_{c_i} represents the direction vector perpendicular from the point of contact to the center of the head cone of forces, it follows that the equations that govern the kinematics of the IAB continuum are given as (see derivation in Appendix § C)

$$\begin{aligned}\sigma_{rr}(R) &= -\int_{R_i}^{R_\circ} \frac{1}{r}(\sigma_{\theta\theta} + \sigma_{\phi\phi} - 2\sigma_{rr})\frac{dr}{dR}dR, \\ &= -\int_{R_i}^{R_\circ} \left[2C_1\left(\frac{1}{r} - \frac{R^6}{r^7}\right) - 2C_2\left(\frac{R^4}{r^5} - \frac{r}{R^2}\right)\right] dR,\end{aligned} \tag{14}$$

and

$$\begin{aligned}P(r) &= \int_{r_i}^{r_\circ} \left[2C_1\left(\frac{r}{R^2} - \frac{R^4}{r^5}\right) + 2C_2\left(\frac{r^3}{R^4} - \frac{R^2}{r^3}\right)\right] dr \\ P(R) &\equiv \int_{R_i}^{R_\circ} \left[2C_1\left(\frac{1}{r} - \frac{R^6}{r^7}\right) - 2C_2\left(\frac{R^4}{r^5} - \frac{r}{R^2}\right)\right] dR.\end{aligned} \tag{15}$$

B. Contact Forces, IAB Stress Components, and Head Gravitational Force

Here, we relate the microscopic contact stress of the previous section with the macroscopic descriptions of the contact friction to enable us treat different material combinations for the manipulator and head. We assume that the stress vector $\boldsymbol{\sigma}$ at a point on the IAB surface is uniform and continuous throughout the IAB boundary so that it linearly depends on the normal map (this follows from Cauchy's theorem; readers may see the proof in [22, §3.3.1]). Recall that the correspondence between material line, $\{\mathbf{dx}, \mathbf{dX}\}$, elements in the reference and current configuration is

$$\mathbf{dx} = \mathbf{F}\ \mathbf{dX} \quad \Longrightarrow \quad \mathbf{F}^{-T}\mathbf{dx} = \mathbf{dX}. \tag{16}$$

where $\mathbf{F}$ is the deformation gradient. Let $\mathbf{H} = \mathbf{F}^{-T}$ and $\mathbf{dA}$ represent an infinitesimal vector element on the material surface at a neighborhood of point $\mathbf{X}$ in $\mathscr{B}$ such that $\mathbf{dA} = \mathbf{N}$dA, where $\mathbf{N}$ is the unit outward normal to the IAB boundary $\partial\mathscr{B}_\circ$ in the reference configuration. The corresponding deformed surface of the IAB with normal $\mathbf{n}$ from a surface, da, of the IAB in the current configuration is $\mathbf{da} = \mathbf{n}\,\mathrm{da}$. Using *Nanson's formula*, we have the following relation between surfaces in the reference and current configuration

$$\mathbf{da} = J\,\mathbf{H}\ \mathbf{dA} \quad \Longrightarrow \quad \mathbf{n}\,\mathrm{da}\ = J\,\mathbf{H}\ \mathbf{N}\ \mathrm{dA}. \tag{17}$$

where $J = \det \mathbf{F}$. Multiplying throughout equation (17) by the derived constitutive relation between the stress-strain relationship of [1], the resultant contact force on the boundary $\partial\mathcal{B}$ in the current configuration may be written as (owing to the volume preservation on the boundary of the IAB material)

$$\int_{\partial\mathscr{B}} \boldsymbol{\sigma}\,\mathbf{n}\,\mathrm{da} = \int_{\partial\mathscr{B}_\circ} J\,\boldsymbol{\sigma}\,\mathbf{H}\,\mathbf{N}\ \mathrm{dA}. \tag{18}$$

We may define the *Piola-Kirchoff* stress tensor field as

$$\mathbf{S} = J\,\mathbf{H}^T\,\boldsymbol{\sigma} \tag{19}$$

so that the force on an element surface da of the IAB in a configuration $\mathscr{B}$ is

$$\boldsymbol{\sigma}\mathbf{da} = \mathbf{S}^T\mathbf{dA}.$$

Thus, the contact force f_{c_i} on the boundary $\partial\mathscr{B}$ of the i^{th} IAB in a configuration $\mathscr{B}$ (as in (9)) is

$$f_{c_i} = \mathbf{S}_i^T\mathbf{dA}_i = J_i\boldsymbol{\sigma}_i\mathbf{H}_i\mathbf{dA}_i = J_i\boldsymbol{\sigma}_i\mathbf{F}_i^{-1}\mathbf{dA}_i \tag{20}$$

where (20) follows from the symmetric property of $\mathbf{F}_i$ and $\boldsymbol{\sigma}_i$. For the i^{th} IAB, at the region of contact, we have the contact force as

$$f_{c_i} = J_i\left(\frac{R_i^2}{r_i^2}P_i + \frac{R_i}{r_i}\sigma_{\phi\phi_i}(\epsilon) + \frac{R_i}{r_i}\sigma_{\theta\theta_i}(\zeta)\right)\mathbf{dA}_i \tag{21}$$

where $\sigma_{jj_i}(\upsilon)$ are the definite integrals of (**??**). Owing to the isochoric deformation assumption, we have from (21) that

$$f_{c_i} = \left(\frac{R_i^2}{r_i^2}P_i + \frac{R_i}{r_i}\sigma_{\phi\phi_i}(\epsilon) + \frac{R_i}{r_i}\sigma_{\theta\theta_i}(\zeta)\right)n_{c_i}dA_i. \tag{22}$$

where we have set the outward normal map $\mathbf{N}$ to n_{c_i} of (9). The torque is the moment of the contact force on the i^{th} IAB,and it is given by

$$\boldsymbol{\tau}_{c_i} = f_{c_i} \times r_{c_i} \tag{23}$$

where $r_{c_i} \in \mathbb{R}^3$ is the unit vector between the head reference point and the contact. The soft contact force of (9) can be re-stated in terms of the derived stress tensor, the deformation

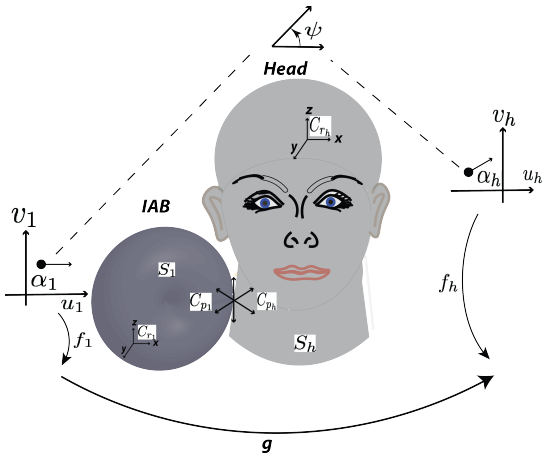

Fig. 5. Sliding and rolling contact illustration of a single IAB and the Head. [Image best visualized in colored ink].

gradient (see [1]) and the Piola-Kirchoff stress field of (19) *i.e.*

Friction Cones' Contact Force

$$\tilde{F}_{c_i} = \begin{bmatrix} \mathbf{I} & 0 \\ 0 & n_{c_i} \end{bmatrix} \begin{bmatrix} f_{c_i} \\ f_{c_i} \times r_{c_i} \end{bmatrix}. \tag{24}$$

where f_{c_i} and $\boldsymbol{\tau}_{c_i}$ are as given in equations (22) and (23).

C. Contact Coordinates and Head Velocity

The head will make contact with the IAB at multiple points on its surface, so we describe the kinematics of these contact points using an atlas[4] of contact coordinate charts. In this sentiment, let C_{r_1} and C_{r_h} respectively represent a fixed reference frame with respect to the IAB and head, H (see Figure 5). Furthermore, let $S_1 \subset \mathbb{R}^3$ and $S_h \subset \mathbb{R}^3$ denote the respective *orientable manifold*[5] embeddings of the IAB and head surfaces with respect to frames C_{r_1} and C_{r_h}. We shall let S_1 and S_r belong to the *atlases* $\{S_{1_i}\}_{i=1}^{n_1}$, $\{S_{h_i}\}_{i=1}^{n_r}$ respectively. Suppose (f_1, U_1) and (f_r, U_r) are *coordinate systems* for the IAB and the head respectively, where f_i is an invertible map, $f_i(u_i, v_i) : U \to S_i \subset \mathbb{R}^3$

$$f_i(u_i, v_i) : \{U \to S_i \subset \mathbb{R}^3 | i = 1, h\},$$

from an open subset U of $\mathbb{R}^2$ to a *coordinate patch* $S_i \subset \mathbb{R}^3$ such that the partial derivatives $\frac{\partial f_i}{\partial u_i}$ and $\frac{\partial f_i}{\partial v_i}$ are linearly independent. Let $p_1(t) \in S_1$ and $p_h(t) \in S_h$ represent the positions of the contact points with respect to frames C_{r_1} and C_{r_h} respectively at time t. In general, the contact points $p_1(t)$ and $p_h(t)$ will not remain in the coordinate systems S_1 and S_h for all time. Thus, we choose an interval I where $p_1(t) \in S_{1_i}$ and $p_h(t) \in S_{h_j}$ for all $t \in I$ and some i and j. As seen in Figure 5, C_{p_1} and C_{p_h} denote the contact frames that coincide with the *normalized Gauss frames* at p_1 and p_h for all $t \in I$, and α_1, α_h are local coordinate frames that describe the IAB motion with respect to the head such that

$$\alpha_1 = (u_1, v_1) \in U_1, \text{ and } \alpha_h = (u_h, v_h) \in U_h. \tag{25}$$

Let the angle between the tangent planes of α_1, and α_h be ψ. The transformation matrix $g \in \Omega \subset SE(3)$ encodes the relative orientation and position of the IAB with respect to the head where Ω is the set of all relative positions and orientations in the atlasses $\{S_{1_i}\}_{i=1}^{n_1}$, $\{S_{h_i}\}_{i=1}^{n_h}$ for which the IAB and head remain in contact. We let the *contact coordinates* be described by $\eta = (\alpha_1, \alpha_h, \psi)$. The head's motion is governed by traction forces arising from the friction tangential to the IAB surface and the pressure normal to the IAB surface. Thus, at the points of contact, if $R \in SO(3)$ is the rotatory component of g, η must satisfy

$$g \circ f_1(\alpha_1) = f_h(\alpha_h) \tag{26a}$$
$$R\, n_1(\alpha_1) = -n_h(\alpha_h) \tag{26b}$$

since the contact locations must coincide for the IAB and the head, and the tangent planes must coincide so that the outward normal maps $n_1 : S_1 \to S^2 \subset \mathbb{R}^3$ and $n_h : S_h \to S^2 \subset \mathbb{R}^3$ agree. Furthermore, the orientation of the tangent planes of α_1 and α_h is the unique angle $\psi \in [0, 2\pi)$ between the x-axes of C_{p_1} and C_{p_h} such that

$$R \frac{\partial f_1}{\partial \alpha_1} M_1^{-1} R_\psi = \frac{\partial f_h}{\partial \alpha_h} M_h^{-1} \tag{27}$$

where M_i is a 2×2 square root of the Riemannian metric tensor [33] that normalizes the columns of $\frac{\partial f}{\partial \alpha}$, *i.e.*

$$M_i = \begin{bmatrix} \|\frac{\partial f_i}{\partial u_i}\| & 0 \\ 0 & \|\frac{\partial f_h}{\partial v_i}\| \end{bmatrix} \tag{28}$$

and R_ψ is chosen such that a rotation of C_{p_1} about its z-axis through $-\psi$ radians aligns the x-axes of the local coordinate system α_1 to that of the head's local coordinate system α_h *i.e.*

$$R_\psi = \begin{bmatrix} \cos\psi & -\sin\psi \\ -\sin\psi & -\cos\psi, \end{bmatrix} \tag{29}$$

with the special property that $R_\psi = R_\psi^T = R_\psi^{-1}$. We define the normalized Gauss frame at a point u on the surface U of the orthogonal coordinate system (f, U) as,

$$\begin{bmatrix} x_u & y_u & z_u \end{bmatrix} = \begin{bmatrix} \frac{\partial f}{\partial u}/\|\frac{\partial f}{\partial u}\| & \frac{\partial f}{\partial v}/\|\frac{\partial f}{\partial v}\| & n_u(f(u)) \end{bmatrix} \tag{30}$$

where x_u, y_u, and z_u are functions mapping $U \subset \mathbb{R}^2 \to \mathbb{R}^3$ and n_u is the continuous Gauss map $n_u : S \to S^2 \subset \mathbb{R}^3$. The motion of the contacts $\dot{\eta}$ as a function of components of the twist vector $\hat{\xi} = (v, w)^T$ is given in (31) as the respective *first, second*, and *third equations of contact*. Our derivation, which closely follows [34]'s multi-fingered kinematics' proof, may be found in Appendix B.

$$\dot{\alpha}_h = M_h^{-1}(\mathcal{K}_h + \tilde{\mathcal{K}}_1)^{-1}\left(\omega_t - \tilde{\mathcal{K}}_1 v_t\right) \tag{31a}$$
$$\dot{\alpha}_1 = M_1^{-1} R_\psi (\mathcal{K}_h + \tilde{\mathcal{K}}_1)^{-1}(\omega_t - \mathcal{K}_h v_t) \tag{31b}$$
$$\dot{\psi} = \omega_n + T_h M_h \dot{\alpha}_h + T_1 M_1 \dot{\alpha}_1 \tag{31c}$$

[4] An atlas $\tilde{S}$ is a set of surfaces where each surface $S \in \tilde{S}$ has an invertible map $f(\boldsymbol{u})$ from an open subset U of $\mathbb{R}^2$ to a surface $S \subset \mathbb{R}^3$ such that the partial derivatives $\frac{\partial f}{\partial u}(\boldsymbol{u})$, $\frac{\partial f}{\partial v}(\boldsymbol{v})$ are linearly independent for all $\boldsymbol{u} = (u, v) \in U$.

[5] An orientable manifold is a manifold S for which the Gauss map exists.

where

$$
\begin{aligned}
T_h &= y_h^T \frac{\partial x_h}{\partial \alpha_h} M_h^{-1}, \quad T_1 = y_1^T \frac{\partial x_1}{\partial \alpha_1} M_1^{-1}, \\
\mathcal{K}_h &= \begin{bmatrix} x_h^T, & y_h^T \end{bmatrix}^T \frac{\partial n_h^T}{\partial \alpha_h} M_h^{-1}, \quad \omega_n = z_h^T \omega \\
\mathcal{K}_1 &= R_\psi \begin{bmatrix} x_1^T, & y_1^T \end{bmatrix}^T \frac{\partial n_1^T}{\partial \alpha_1} M_1^{-1} R_\psi, \\
\omega_t &= \begin{bmatrix} x_h^T, & y_h^T \end{bmatrix}^T \begin{bmatrix} n_h \times \omega \end{bmatrix}^T, \\
v_t &= \begin{bmatrix} x_h^T, & y_h^T \end{bmatrix}^T \begin{bmatrix} (-f_h \times \omega + v) \end{bmatrix}^T. \qquad (32)
\end{aligned}
$$

Note that ω_t is the rolling velocity of the head projected onto the tangent plane of the contact and v_t is the sliding velocity; ω_n is the relative rotational velocity projected to the contact's surface normal, and $\tilde{\mathcal{K}}_1 = R_\psi \mathcal{K}_1 R_\psi$ is the curvature of the IAB with respect to the contact frame that coincides with the normalized Gauss frame at $p_1(t)$. The matrix $(\mathcal{K}_h + \tilde{\mathcal{K}}_1)^{-1}$ is the so-called *relative curvature* originally coined by [31]. Simplifying (32), we find that

$$
\begin{aligned}
x_h &= \frac{\partial f}{\partial u_h} / \| \frac{\partial f}{\partial u_h} \|, \quad y_h = \frac{\partial f}{\partial v_h} / \| \frac{\partial f}{\partial v_h} \|, \qquad z_h = n_u(f(u)) \\
T_h &= y_h \left[\frac{\partial x_h^T}{\partial u_h} / \| \frac{\partial f}{\partial u_h} \|, \frac{\partial x_h^T}{\partial v_h} / \| \frac{\partial f}{\partial v_h} \| \right], \\
T_1 &= y_1 \left[\frac{\partial x_1^T}{\partial u_1} / \| \frac{\partial f}{\partial u_1} \|, \frac{\partial x_1^T}{\partial v_1} / \| \frac{\partial f}{\partial v_1} \| \right], \\
\mathcal{K}_h &= \begin{bmatrix} x_h^T, & y_h^T \end{bmatrix}^T \left[\frac{\partial n_h^T}{\partial u_h} / \| \frac{\partial f}{\partial u_h} \|, \frac{\partial n_h^T}{\partial v_h} / \| \frac{\partial f}{\partial v_h} \| \right], \\
\mathcal{K}_1 &= \begin{bmatrix} x_1^T, & y_1^T \end{bmatrix}^T \left[\frac{\partial n_1^T}{\partial u_1} / \| \frac{\partial f}{\partial u_1} \|, \frac{\partial n_1^T}{\partial v_1} / \| \frac{\partial f}{\partial v_1} \| \right]. \qquad (33)
\end{aligned}
$$

This is verified in Appendix C. We see that for the contact interaction between an IAB and the head, for a $U \subset \mathbb{R}^2$ we must choose an appropriate $f_i : U_i \to S_i \subset \mathbb{R}^3$ in order to characterize the setup.

VI. System's Newton-Euler Equations

From Truesdell's *determinism for the stress principle* [35], the Cauchy stress $\boldsymbol{\sigma}$ at any point in a material at time t for any motion up to time t determines the stress response of the material for any arbitrary motion history up to and including time t. We will derive the dynamics of the IAB system in the *strain field of the deformation*. The potential and kinetic energy of the system are considered to be derived from the constitutive strain field relations that characterize the deformation. We now use Lagrangian deformation analysis to derive the dynamic equations of the continuum multi-IAB system.

For a soft continuum body, there is an enormous amount of particle orientations during deformation; the number of particle states that is physically measurable with sensors instantaneously in a given configuration is overwhelming. However, we can leverage the constitutive law which describes the macroscopic IAB material behavior with respect to a reference frame, S, at a time, t by completely characterizing it by ten dependent variables viz., three components of the position vector, six component stress tensor variables (the shear and normal stress components), and

A. Lagrangian and Euler-Lagrange Equations

Following § IV, we are only interested in the final position and orientation of the IAB as a whole rather than the system of particles that characterize a deformation at every time t.When the head exerts a reactive wrench on an IAB, it is natural to expect a dent. The shear angle in (8) should capture the amount of angular deformation. For a kinetic energy T and a potential energy V, the *Lagrangian,* L, of the system in generalized coordinates is the difference between the kinetic and potential energy, $i.e.$

$$
L(\mathbf{r}, \dot{\mathbf{r}}) = T(\mathbf{r}, \dot{\mathbf{r}}) - V(\mathbf{r}). \qquad (34)
$$

The equations of motion for a pneumatic IAB system is of the form

$$
\frac{d}{dt} \frac{\partial L}{\partial \dot{\mathbf{r}}_i} - \frac{\partial L}{\partial \mathbf{r}_i} = \boldsymbol{\tau}_i, \quad i = 1, \ldots, m \qquad (35)
$$

where $\boldsymbol{\tau}_i$ is the torque acting on the i^{th} generalized coordinate. Written in matrix form equation, we can write the Euler-Lagrange equation of (35) as

$$
\frac{d}{dt} \frac{\partial L}{\partial \dot{\mathbf{r}}} - \frac{\partial L}{\partial \mathbf{r}} = \boldsymbol{\tau}. \qquad (36)
$$

It now remains to derive the kinetic and potential energies for the IAB material. Let the velocity of an IAB material particle $\mathbf{x}$ in the current configuration at time t be $\mathbf{v}(\mathbf{r}, t)$, then the Eulerian velocity gradient tensor can be defined as

$$
\boldsymbol{\Gamma} = \text{grad } \mathbf{v}(\mathbf{r}, t). \qquad (37)
$$

Cauchy's first law of motion (**??**) will allow us to derive the balance of mechanical energy of the system. Multiplying(**??**) throughout by $\mathbf{v}(\mathbf{r}, t)$, and abusing notation by dropping the arguments of $\mathbf{v}(\mathbf{r}, t)$, we find that

$$
\begin{aligned}
&\text{div } (\boldsymbol{\sigma}^T \cdot \mathbf{v}) + \rho \mathbf{b} \cdot \mathbf{v} = \rho \mathbf{v} \cdot \dot{\mathbf{v}} \\
\implies &\text{div } (\boldsymbol{\sigma}^T \mathbf{v}) - \mathbf{tr}(\boldsymbol{\sigma}\, \boldsymbol{\Gamma}) + \rho \mathbf{b} \cdot \mathbf{v} = \rho \mathbf{v} \cdot \dot{\mathbf{v}}. \qquad (38)
\end{aligned}
$$

where ρ is the mass density of the IAB material body. Following mass conservation, we integrate over volume $\mathscr{B}$ and employ the divergence theorem, so that the above relation yields the *balance of mechanical energy*:

$$
\int_{\mathscr{B}} \rho \mathbf{b} \cdot \mathbf{v}\, dv + \int_{\partial \mathscr{B}} f_\rho \cdot \mathbf{v}\, da = \frac{d}{dt} \int_{\mathscr{B}} \frac{1}{2} \rho \mathbf{v} \cdot \mathbf{v}\, dv + \int_{\mathscr{B}} \mathbf{tr}(\boldsymbol{\sigma}\, \boldsymbol{\Gamma})\, dv \qquad (39)
$$

where f_ρ is the IAB body force density, and the left hand side of the foregoing is the so-called *rate of working of the applied forces*. The symmetry of the stress tensor $\boldsymbol{\sigma}$ implies that $\mathbf{tr}(\boldsymbol{\sigma}\, \boldsymbol{\Gamma}) = \mathbf{tr}(\boldsymbol{\sigma}\, \boldsymbol{\Sigma})$ where $\boldsymbol{\Sigma}$ is given in terms of the Eulerian-strain rate tensor, Γ $i.e.$

$$
\boldsymbol{\Sigma} = \frac{1}{2} (\boldsymbol{\Gamma} + \boldsymbol{\Gamma}^T) \qquad (40)
$$

so that the kinetic energy density and stress power are given by,

$$
T(\mathbf{r}, \dot{\mathbf{r}}) = \frac{1}{2} \rho \mathbf{v} \cdot \mathbf{v}, \quad V(\mathbf{r}) = \mathbf{tr}(\boldsymbol{\sigma}\, \boldsymbol{\Sigma}). \qquad (41)
$$

B. Case I: Euler-Lagrange Equation for Cauchy-Elastic IAB Material

The stress-strain relation for the IAB we have presented are only related through the deformation tensor, implying that the material is Cauchy elastic. For Cauchy elastic materials, the stress power term is not conserved during deformation making integration over the material body $\mathscr{B}$ physically unrealistic [22]. For such materials, we may set the stored strain energy V to an arbitrary constant (e.g. an identity or $V(I) = 0$). We can derive the overall torque dynamics of an IAB system as (see proof in Appendix A)

$$\boldsymbol{\tau} = \underbrace{\begin{bmatrix} \rho/R^2 & 0 & 0 \\ 0 & 9\rho r_i^4/2 & 0 \\ 0 & 0 & \rho \end{bmatrix}}_{M_{iab}} \ddot{\mathbf{r}} + \underbrace{\begin{bmatrix} \rho\dot{r}/R^3 & 0 & 0 \\ 0 & 36\rho r_i^3 \dot{r}_i & 0 \\ 0 & 0 & 0 \end{bmatrix}}_{C_{iab}} \dot{\mathbf{r}} \tag{42}$$

Rewriting equation (42) in terms of the torque for each soft robot, we have the dynamics for IAB j as

$$M_{iab^j}(\mathbf{r}^j)\ddot{\mathbf{r}}^j + C_{iab^j}(\mathbf{r}^j, \dot{\mathbf{r}}^j)\dot{\mathbf{r}}^j = \boldsymbol{\tau}^j \tag{43}$$

where M_{iab^j} and C_{iab^j} contain the respective inertia and Coriolis forces for actuator j. Since the IAB material is incompressible, the mass density is uniform throughout the body of the material. In general, we write equation (43) as

$$\boldsymbol{M}_{iab}(\tilde{\mathbf{r}})\ddot{\tilde{\mathbf{r}}} + \boldsymbol{C}_{iab}(\tilde{\mathbf{r}}, \dot{\tilde{\mathbf{r}}})\dot{\tilde{\mathbf{r}}} = \tilde{\boldsymbol{\tau}} \tag{44}$$

where $\tilde{\mathbf{r}} \in \mathbb{R}^{n_1} \times \mathbb{R}^{n_2} \times \cdots \mathbb{R}^{n_8}$ gives the generalized coordinates for all the IABs and $\tilde{\boldsymbol{\tau}}$ are the vectorized torques of the individual robots.

C. Case II: Euler-Lagrange Equation for Green Elastic IAB Material

For the case where the IAB material body is *Green elastic* or *hyperelastic*[6], the eulerian form of the stress power expression is

$$V(\mathbf{r}) = \mathbf{tr}(\boldsymbol{\sigma}\, \boldsymbol{\Sigma}). \tag{45}$$

We are mostly interested in the mechanical energy in the current configuration, however, it is worthwhile to note that the equivalent relation in the Lagrangean form is

$$\int_{\mathscr{B}_\circ} \rho_\circ \mathbf{b}_\circ \dot{\boldsymbol{\chi}}\, dV + \int_{\partial\mathscr{B}_\circ} (\mathbf{S}^T\mathbf{N})\dot{\boldsymbol{\chi}}\, dA = \frac{d}{dt}\int_{\mathscr{B}_\circ} \frac{1}{2}\rho_\circ\, \dot{\boldsymbol{\chi}} \cdot \dot{\boldsymbol{\chi}}\, dV + \int_{\mathscr{B}_\circ} \mathbf{tr}(\mathbf{S}\dot{\mathbf{F}})\, dV, \tag{46}$$

where $\mathbf{S}$ is the Piola-Kirchoff stress tensor. It follows that,

$$V(\mathbf{r}) = \mathbf{tr}(\mathbf{S}\dot{\mathbf{F}}) \tag{47}$$

for a Green elastic material. Similar to the arguments in § VI-B, we find the torque as (see derivation in Appendix A)

[6]An hyperelastic material is one where the strain-energy function exists.

Green-Elastic IAB Material Torque

$$\boldsymbol{\tau} = \frac{\rho\ddot{r}}{R^2} + 9\rho r_i^4 \ddot{r}_i + \rho\ddot{\alpha} + \frac{\rho\dot{r}^2}{R^3} + 36\rho r_i^3 \dot{r}_i^2 + 4C_1\left(\frac{2R^3}{r^5} + \frac{r}{R^3}\right) + 4C_2\left(\frac{2r^3}{R^5} + \frac{R}{r^3}\right). \tag{48}$$

whereupon the equation may be vectorized as in (44).

VII. Multi-IAB Statics and End-Effector Velocities

At a material point, $\mathbf{r}$, of the IAB surface in the configuration $\mathscr{B}$, the 3D position of a point is given by (**??**). Since deformation is radially symmetric, it follows that the regularity of the IAB in its current configuration, $\boldsymbol{\chi}(\mathbf{r}, t)$, implies that it can be uniformly defined by $\mathbf{r}$ throughout the IAB material body. Similar to [1], we are interested in the final state of the IAB after deformation; the path it takes for us to reach the final configuration is not important to us (since there is no obstacle in the continuum robots' workspace). Thus we drop the time dependence on the configuration and take $\mathbf{r}$ to be the generalized coordinate of the IAB. The configuration space of the IAB with respect to the spatial frame at a certain time can then be described by $g_{st}(\boldsymbol{\chi}) \equiv g_{st}(\mathbf{r}) : \mathbf{r} \to g_{st}(\mathbf{r}) \in SE(3)$ while the strain state of the IAB is characterized by the strain field

$$\hat{\xi}_i(\mathbf{r}) = g_i^{-1}\frac{\partial g_i}{\partial \mathbf{r}} \in \mathfrak{se}(3) = g_i^{-1} g_i' \tag{49}$$

with the respective g_i's being the tangent vector at g_i such that $g_i' \in T_{g_i(\mathbf{r})}SE(3)$. Note that $T_{g_i(\mathbf{r})}$ is the tangent matrix at g_i with associated Lie algebra $se(3) \approx T_e SE(3)$.

A. End Effector Forces

From the derived relationship between the head contact coordinates and the relative motion (v_t, ω_t) of the IAB *i.e.* equation (31), we can associate a Jacobian that maps IAB velocities to head position and orientation. A fundamental assumption in our formulation is that the IABs make contact with the head throughout manipulation, and the manipulation is stable and prehensile. A forward kinematic map from the configuration of the $i'th$ IAB, $\boldsymbol{\chi}_{iab_i}$ maps from respective IAB configurations to head position and orientation *i.e.* $K_{iab_i} : \boldsymbol{\chi}_{iab_i} \to SE(3)$. The velocity of the head with respect to a fixed base frame in terms of IAB velocities can be written in terms of the forward kinematics Jacobian:

$$\begin{pmatrix} v_{iab_i} \\ \omega_{iab_i} \end{pmatrix} = \frac{\partial K_{iab_i}}{\partial \mathbf{r}_i}\frac{d\mathbf{r}}{dt} K_{iab_i}^{-1} = \boldsymbol{J}_i(\mathbf{r}_i)\dot{\mathbf{r}}_i \tag{50}$$

where $\mathbf{r}_i$ is the spatial position of IAB i, and $(v_{iab_i}^T, \omega_{iab_i}^T) \in \mathbb{R}^6$ represents the linear and angular velocity of the i^{th} IAB about its screw basis. In essence, $\mathbf{r}_i \in \mathbb{R}^3$ with its rows of mapped to scalars by an appropriate choice of norm. The contact between the head and the IABs is mapped by the Jacobian

$$\boldsymbol{J}_{c_i}(\xi_h, \xi_{iab_i}) = \begin{bmatrix} \mathbf{I} & \hat{\boldsymbol{w}}(r_{c_i}) \\ \mathbf{0} & \mathbf{I} \end{bmatrix} J_{r_i}, \tag{51}$$

where $\boldsymbol{J}_{c_i} : \dot{\xi}_{r_i} \to \begin{bmatrix} v_{c_i}^T, & w_{c_i}^T \end{bmatrix}^T$, $r_{c_i} \in \mathbb{R}^3$ is a vector between the head reference point (e.g. the center of mass) and the contact with the i^{th} IAB, ξ_h is the position and relative orientation of the head, ξ_{iab_i} is the position and relative orientation of the i^{th} soft robot in world coordinates, $\hat{\boldsymbol{w}}(r_{c_i})$ is an anti-symmetric matrix for the vector r_{c_i}, and $\xi_r = (\xi_{r_1}, \xi_{r_2}, \cdots, \xi_{r_8})$ are the positions and orientations for each of the 8 IABs. The manipulation map, G_i is made up of matrices of the form

$$G_i(\xi_h, \xi_r) = \begin{bmatrix} \mathbf{I} & \mathbf{0} \\ \hat{w}(r_{c_i}) & \mathbf{I} \end{bmatrix} B_i(\xi_h, \xi_r), \tag{52}$$

where $B_i(\xi_h, \xi_r)$ is the selection map as defined in [36] for the desired manipulation. The net force on the head is a sum of the individual forces arising from each IAB. Owing to the linearity of each individual IAB's contact force, the resultant head force can be stitched together to form G, $i.e.$

$$\tilde{F}_h = \begin{bmatrix} G_1, \ldots, G_8 \end{bmatrix} \begin{pmatrix} \tilde{F}_{c_1} \\ \vdots \\ \tilde{F}_{c_8} \end{pmatrix} = G\tilde{F}_c, \tag{53}$$

where $F_h \in \mathbb{R}^6$ and $F_c \in \mathbb{R}^{m_1} \times \mathbb{R}^{m_2} \times \ldots \times \mathbb{R}^{m_8}$. The *internal* or *null forces* is captured by the null space $\mathcal{N}(G)$ of the manipulation map G; these forces correspond to zero net force on the head of the patient. Each $\tilde{F}_{c_i}$ in (53) is of the form (24).

B. End-effector Velocities

We define the velocity constraint dual of (52) as the constraint between the relative velocity of the head and that of the twist velocities of the contact point

$$\begin{pmatrix} \tilde{v}_{c_i} \\ \tilde{\omega}_{c_i} \end{pmatrix} = \begin{bmatrix} \mathbf{I} & \hat{\omega}(r_{c_i}) \\ 0 & \mathbf{I} \end{bmatrix} \begin{pmatrix} v_{c_h} \\ \omega_{c_h} \end{pmatrix}. \tag{54}$$

For a conjugate twist vector $(v_c^T, \omega_c^T)^T$ to the forces exerted by the IABs, f_c, we have the following

$$\begin{pmatrix} v_c \\ \omega_c \end{pmatrix} = G^T \begin{pmatrix} v_{c_h} \\ \omega_{c_h} \end{pmatrix}. \tag{55}$$

Given a *selection matrix* $B_i^T(\xi_h, \xi_{iab_i}) \in \mathbb{R}_i^m$ for a particular IAB, where m_i is the range of all the forces and moments for the chosen contact primitive (or union of contact primitives), the *manipulation map* for the i^{th} IAB can be written as,

$$G_i^T(\xi_h, \xi_{iab_i})\xi_h = B_i^T(\xi_h, \xi_{iab_i})\boldsymbol{J}_{c_i}(\xi_h, \mathbf{r}_{r_i})\dot{\xi}_{iab_i} \tag{56}$$

where $\boldsymbol{J}_{c_i}$ is the contact Jacobian for the i^{th} actuator, and ξ_h denotes the velocity of the head. For the 8 soft actuators, the manipulation constraint of the system can be written as

$$\begin{bmatrix} G_1^T \\ G_2^T \\ \vdots \\ G_8^T \end{bmatrix} \begin{pmatrix} v_h \\ w_h \end{pmatrix} = \mathbf{diag} \begin{pmatrix} B_1^T \boldsymbol{J}_{c_1} \\ B_2^T \boldsymbol{J}_{c_2} \\ \vdots \\ B_8^T \boldsymbol{J}_{c_8} \end{pmatrix} \begin{pmatrix} \dot{\mathbf{r}}_{iab_1} \\ \dot{\mathbf{r}}_{iab_2} \\ \vdots \\ \dot{\mathbf{r}}_{iab_8} \end{pmatrix}. \tag{57}$$

VIII. Newton-Euler System of Equations

The dynamics of the head is a form of (44) but without the actuator torques. In local coordinates, it has the form

$$\boldsymbol{M}_h(\zeta)\ddot{\zeta} + \boldsymbol{C}_h(\zeta, \dot{\zeta})\dot{\zeta} + \boldsymbol{N}_h(\zeta, \dot{\zeta}) = 0 \tag{58}$$

with ζ being a local parameterization of the position and orientation of the head in the Lie Group $SE(3)$, and $\boldsymbol{N}_h$ being the gravitational and frictional forces exerted by/on the head. The head and the multi-DOF IAB system are connected via the manipulation constraint $i.e.$

$$G^T(\zeta, \mathbf{r})\dot{\zeta} = \boldsymbol{J}(\zeta, \mathbf{r})\dot{\mathbf{r}}. \tag{59}$$

Suppose that the velocity constraint produces a virtual displacement constraint in $\delta\zeta$ and $\delta\mathbf{r}$ such that for $q = (\zeta, \mathbf{r})$, we have

$$\delta\mathbf{r} = \boldsymbol{J}^{-1}(q)G^T(q)\delta\zeta$$

the Lagrange equations become

$$\left(\frac{d}{dt}\frac{\partial L}{\partial \dot{q}} - \frac{\partial L}{\partial q} - (\boldsymbol{\tau}, 0)\right)\delta q = 0 \tag{60a}$$

$$\begin{pmatrix} \frac{d}{dt}\frac{\partial L}{\partial \dot{\mathbf{r}}} - \frac{\partial L}{\partial \mathbf{r}} - \boldsymbol{\tau} \\ \frac{d}{dt}\frac{\partial L}{\partial \dot{\zeta}} - \frac{\partial L}{\partial \zeta} \end{pmatrix}^T \begin{pmatrix} \delta\mathbf{r} \\ \delta\zeta \end{pmatrix} = 0 \tag{60b}$$

$$\left(\frac{d}{dt}\frac{\partial L}{\partial \dot{\mathbf{r}}} - \frac{\partial L}{\partial \mathbf{r}} - \boldsymbol{\tau}\right)\delta\mathbf{r} + \left(\frac{d}{dt}\frac{\partial L}{\partial \dot{\zeta}} - \frac{\partial L}{\partial \zeta}\right)\delta\zeta = 0 \tag{60c}$$

$$GJ^{-T}\left(\frac{d}{dt}\frac{\partial L}{\partial \dot{\mathbf{r}}} - \frac{\partial L}{\partial \mathbf{r}} - \boldsymbol{\tau}\right)\delta\zeta + \left(\frac{d}{dt}\frac{\partial L}{\partial \dot{\zeta}} - \frac{\partial L}{\partial \zeta}\right)\delta\zeta = 0 \tag{60d}$$

wherefore,

$$\left(\frac{d}{dt}\frac{\partial L}{\partial \dot{\zeta}} - \frac{\partial L}{\partial \zeta}\right)\delta\zeta + GJ^{-T}\left(\frac{d}{dt}\frac{\partial L}{\partial \dot{\mathbf{r}}} - \frac{\partial L}{\partial \mathbf{r}}\right) = GJ^{-T}\boldsymbol{\tau} \tag{61}$$

given the arbitrariness of $\delta\zeta$. Equations (61) alongside (59) completely describe the system dynamics. Putting (43) into (61), we have

$$\left(\frac{d}{dt}\frac{\partial L}{\partial \dot{\zeta}} - \frac{\partial L}{\partial \zeta}\right)\delta\zeta = GJ^{-T}\left(1 - \frac{\rho}{2\|\mathbf{r}\|^2}\right)\boldsymbol{\tau}. \tag{62}$$

IX. Conclusions

We have presented the kinematic motion equations and the Lagrangian dynamics for the mechanism presented in our previous publication. It remains to demonstrate the working examples in closed-loop head motion control. In a follow-up paper to be released shortly, we show how these formulations are applied in real-time on the patient-IAB system.

Appendix A
Robot-Head Dynamics

We now derive the overall dynamics for the elastic IAB in Eulerian form. Following (8), a point on the surface of the IAB has the following description

$$\mathbf{r} = \begin{bmatrix} \lambda \\ r \\ \phi \end{bmatrix} = \begin{bmatrix} r/R \\ (R_\circ^3 + r_i^3 - R_i^3)^{1/3} \\ \beta - \alpha \end{bmatrix} \tag{63}$$

so that the Eulerian time differentiation of $\mathbf{r}$ yields

$$\dot{\mathbf{r}} = \begin{bmatrix}\dot{\lambda}, & \dot{r}, & \dot{\phi}\end{bmatrix}^T = \begin{bmatrix}\dot{r}/R, & 3r_i^2\dot{r}_i, & -\dot{\alpha}\end{bmatrix}^T \tag{64}$$

which follows since $\dot{R} = \dot{\beta} = 0$ in the reference configuration. Similarly, we find that $\ddot{\mathbf{r}}$ is given as

$$\ddot{\mathbf{r}} = \begin{bmatrix}\ddot{\lambda}, & \ddot{r}, & \ddot{\phi}\end{bmatrix}^T = \begin{bmatrix}\ddot{r}/R, & 6r_i{\dot{r}_i}^2 + 3r_i\ddot{r}_i, & -\ddot{\alpha}\end{bmatrix}^T \tag{65}$$

Recall the kinetic energy form of a continuum body (§ VI)

$$T = \frac{1}{2}\rho\mathbf{v}(\mathbf{r},t)\cdot\mathbf{v}(\mathbf{r},t) = \frac{1}{2}\rho\|\dot{\mathbf{r}}\|^2. \tag{66}$$

Given the incompressibility of the IAB material body, the material mass density is uniform throughout the body at a configuration so that the rate of change of of the body mass, ρ, vanishes.

A. Case I: Cauchy Elastic IAB Material Skins

Suppose we choose a Cauchy Elastic material so that the constitutive equation that governs the Cauchy stress tensor, $\boldsymbol{\sigma}$, is independent of the path of the deformation from the reference configuration but is solely a function of the state of deformation. Then, it follows that $V = 0$. We have

$$T = \frac{1}{2}\rho\|\dot{\mathbf{r}}\|^2 = \frac{1}{2}\rho\left(\dot{r}^2/R^2 + 9r_i^4{\dot{r}_i}^2 + \dot{\alpha}^2\right),\ V = 0. \tag{67}$$

It follows that the Lagrangian is

$$L(\mathbf{r},\dot{\mathbf{r}}) = \frac{1}{2}\rho\|\dot{\mathbf{r}}\|^2 = \frac{1}{2}\rho\left(\dot{r}^2/R^2 + 9r_i^4{\dot{r}_i}^2 + \dot{\alpha}^2\right) \tag{68}$$

and the derivatives of the canonical momenta are

$$\frac{d}{dt}\frac{\partial L}{\partial \dot{r}} = \frac{d}{dt}\left(\frac{\rho\,\dot{r}}{R^2}\right) = \rho\left(\frac{\ddot{r}}{R^2} - 2\frac{\dot{r}\dot{R}}{R^3}\right) \equiv \frac{\rho}{R^2}\ddot{r} \tag{69a}$$

$$\frac{d}{dt}\frac{\partial L}{\partial \dot{r}_i} = \frac{d}{dt}\left(9\rho r_i^4\,\dot{r}_i\right) = 9\rho r_i^3\left(4{\dot{r}_i}^2 + r_i\ddot{r}_i\right) \tag{69b}$$

$$\frac{d}{dt}\frac{\partial L}{\partial \dot{\phi}} = \frac{d}{dt}\frac{\partial L}{\partial \dot{\alpha}} = \frac{d}{dt}\left(\rho\dot{\alpha}\right) = \rho\ddot{\alpha}, \tag{69c}$$

where (69a) follows from the fact that the radius is constant in the reference configuration. We therefore have the following associated generalized forces

$$\frac{\partial L}{\partial r} = 0, \frac{\partial L}{\partial R} = -\frac{\rho\dot{r}^2}{R^3} \text{ and } \frac{\partial L}{\partial \phi} = 0. \tag{70a}$$

Recalling the Euler-Lagrange equation from (36), we may write the torque that governs the $j'th$ IAB as (we have dropped the $j'th$ index)

Cauchy-Elastic IAB Material Torque

$$\boldsymbol{\tau} = \frac{\rho\ddot{r}}{R^2} + 9\rho r_i^4\ddot{r}_i + \rho\ddot{\alpha} + \frac{\rho\dot{r}^2}{R^3} + 36\rho r_i^3\dot{r}_i^2 \tag{71}$$

and in matrix form for all the system of IABs, we have

$$\boldsymbol{\tau} = \begin{bmatrix}\rho/R^2 & 0 & 0\\ 0 & 9\rho r_i^4/2 & 0\\ 0 & 0 & \rho\end{bmatrix}\begin{bmatrix}\ddot{r}\\ \ddot{r}_i\\ \ddot{\alpha}\end{bmatrix} + \begin{bmatrix}\dot{r}\\ \dot{r}_i\\ \dot{\alpha}\end{bmatrix}^T\begin{bmatrix}\rho/R^3 & 0 & 0\\ 0 & 36\rho r_i^3 & 0\\ 0 & 0 & 0\end{bmatrix}\begin{bmatrix}\dot{r}\\ \dot{r}_i\\ \dot{\alpha}\end{bmatrix} \tag{72}$$

rewritten compactly as,

$$\boldsymbol{\tau} = \underbrace{\begin{bmatrix}\rho/R^2 & 0 & 0\\ 0 & 9\rho r_i^4/2 & 0\\ 0 & 0 & \rho\end{bmatrix}}_{M_{iab}}\ddot{\mathbf{r}} + \underbrace{\begin{bmatrix}\rho/R^3\dot{r} & 0 & 0\\ 0 & 36\rho r_i^3\dot{r}_i & 0\\ 0 & 0 & 0\end{bmatrix}}_{C_{iab}}\dot{\mathbf{r}} \tag{73}$$

or

$$\boldsymbol{\tau} = M_{iab}(\mathbf{r})\ddot{\mathbf{r}} + C_{iab}(\mathbf{r},\dot{\mathbf{r}})\dot{\mathbf{r}} \tag{74}$$

B. Case II: Green Elastic IAB Material Skins

When the stress tensor depends on the strain, we have from (47), that

$$V(\mathbf{r}) = \mathbf{tr}(\boldsymbol{S}\dot{\mathbf{F}}). \tag{75}$$

The associated force on the head is now a function of the kinetic and potential energies so that we have

$$L(\mathbf{r},\dot{\mathbf{r}}) = \frac{1}{2}\rho\|\dot{\mathbf{r}}\|^2 + \mathbf{tr}(\boldsymbol{S}\dot{\mathbf{F}}) \tag{76a}$$

$$= \frac{1}{2}\rho\left(\dot{r}^2/R^2 + 9r_i^4{\dot{r}_i}^2 + \dot{\alpha}^2\right) + \mathbf{tr}(\boldsymbol{S}\dot{\mathbf{F}}) \tag{76b}$$

$$= \frac{1}{2}\rho\left(\dot{r}^2/R^2 + 9r_i^4{\dot{r}_i}^2 + \dot{\alpha}^2\right) + \mathbf{tr}(J\,\mathbf{H}^T\,\boldsymbol{\sigma}\dot{\mathbf{F}})$$

which follows from (19). We thus have

$$L(\mathbf{r},\dot{\mathbf{r}}) = \frac{1}{2}\rho\left(\dot{r}^2/R^2 + 9r_i^4{\dot{r}_i}^2 + \dot{\alpha}^2\right) + \mathbf{tr}(\mathbf{F}^{-1}\,\boldsymbol{\sigma}\dot{\mathbf{F}}) \tag{77}$$

Recall from [1] that

$$\mathbf{F} = \begin{bmatrix}\frac{R^2}{r^2} & 0 & 0\\ 0 & \frac{r}{R} & 0\\ 0 & 0 & \frac{r}{R}\end{bmatrix} \text{ and } \boldsymbol{\sigma} = C_1\mathbf{B} - C_2\mathbf{C}^{-1} - p\mathbf{I} \tag{78}$$

where C_1 and C_2 are appropriate IAB material moduli, p is the hydrostatic pressure and $\mathbf{B}, \mathbf{C}$ respectively denote the left and right Cauchy-Green deformation tensors. We therefore have the following for the Green-Elastic IAB material Lagrangian

$$L(\mathbf{r},\dot{\mathbf{r}}) = \frac{1}{2}\rho\left(\dot{r}^2/R^2 + 9r_i^4{\dot{r}_i}^2 + \dot{\alpha}^2\right) + \mathbf{tr}(\mathbf{F}^{-1}\,\boldsymbol{\sigma}\dot{\mathbf{F}}) \tag{79}$$

$$= \frac{1}{2}\rho\left(\dot{r}^2/R^2 + 9r_i^4{\dot{r}_i}^2 + \dot{\alpha}^2\right) + 2C_1\left(\frac{R^3}{r^4} - \frac{r^2}{R^3}\right) + 2C_2\left(\frac{R}{r^2} - \frac{r^4}{R^5}\right) \tag{80}$$

where we have taken $\dot{\mathbf{F}}$ is the time derivative of $\mathbf{F}$ with respect to r. Solving for the derivatives of the kinetic and potential energy as before, we have,

$$\frac{d}{dt}\frac{\partial L}{\partial \dot{r}} = \frac{\rho}{R^2}\ddot{r},\ \frac{d}{dt}\frac{\partial L}{\partial \dot{r}_i} = 9\rho r_i^3\left(4{\dot{r}_i}^2 + r_i\ddot{r}_i\right) \tag{81a}$$

$$\frac{d}{dt}\frac{\partial L}{\partial \dot{\phi}} = \rho\ddot{\alpha} \tag{81b}$$

with the following associated generalized forces

$$\frac{\partial L}{\partial r} = -4C_2\left(\frac{2r^3}{R^5} - \frac{R}{r^3}\right) - 4C_1\left(\frac{2R^3}{r^5} - \frac{r}{R^3}\right), \tag{82a}$$

$$\frac{\partial L}{\partial r_i} = 18r_i^3{\dot{r}_i}^2 \text{ and } \frac{\partial L}{\partial \phi} = 0. \tag{82b}$$

We can now write the torque as

Green-Elastic IAB Material Torque

$$\boldsymbol{\tau} = \frac{\rho \ddot{r}}{R^2} + 9\rho r_i^4 \ddot{r}_i + \rho\ddot{\alpha} + \frac{\rho \dot{r}^2}{R^3} + 36\rho r_i^3 \dot{r}_i^2 + 4C_1\left(\frac{2R^3}{r^5} + \frac{r}{R^3}\right) + 4C_2\left(\frac{2r^3}{R^5} + \frac{R}{r^3}\right) \tag{83}$$

Appendix B
Derivation of IAB-Head Contact Kinematics

Here, we formulate the contact kinematics between an IAB and the head in a fashion similar to the single finger soft contact type postulated in [34]. We note that an alternative derivation that is more concise can be found in [31].

A. Contact Coordinates and Gaussian Map

Following equations (26a), (26b), and 27, we write

$$R\, f_1(\alpha_1) + p = f_h(\alpha_h) \tag{84a}$$

$$R\, n_1(\alpha_1) = -n_h(\alpha_h) \tag{84b}$$

$$R\, \frac{\partial f_1}{\partial \alpha_1} M_1^{-1} R_\psi = \frac{\partial f_h}{\partial \alpha_h} M_h^{-1}. \tag{84c}$$

Differentiating (84a) and (84b), we find that

$$\dot{R}\, f_1(\alpha_1) + R\, \frac{\partial f_1}{\partial \alpha_1}\dot{\alpha_1} + \dot{p} = \frac{\partial f_h}{\partial \alpha_h}\dot{\alpha_h} \tag{85}$$

$$\dot{R}\, n_1(\alpha_1) + R\, \frac{\partial n_1}{\partial \alpha_1}\dot{\alpha_1} = -\frac{\partial n_h}{\partial \alpha_h}\dot{\alpha_h}. \tag{86}$$

It follows through the multiplication of (85) by $\frac{\partial f_h}{\partial \alpha_h}^T$ and putting α_h into (86), we have

$$\dot{R}\, n_1(\alpha_1) + R\, \frac{\partial n_1}{\partial \alpha_1}\dot{\alpha_1} = -\frac{\partial n_h}{\partial \alpha_h} M_h^{-2} \frac{\partial f_h}{\partial \alpha_h}^T \left(\dot{R}\, f_1(\alpha_1) + R\, \frac{\partial f_1}{\partial \alpha_1}\dot{\alpha_1} + \dot{p}\right). \tag{87}$$

Now, putting (84c) into (87) and rearranging, we find that

$$\left[R\, \frac{\partial n_1}{\partial \alpha_1} + \frac{\partial n_h}{\partial \alpha_h} M_h^{-2} \left(\frac{\partial f_h^T}{\partial \alpha_h}\frac{\partial f_h}{\partial \alpha_h}\right) M_h^{-1} R_\psi M_1\right]\dot{\alpha}_1 = -\dot{R}\, n_1 - \frac{\partial n_h}{\partial \alpha_h} M_h^{-2} \frac{\partial f_h}{\partial \alpha_h}^T \left(\dot{R}\, f_1(\alpha_1) + \dot{p}\right). \tag{88}$$

Multiplying throughout by $M_h^{-T}\frac{\partial f_h}{\partial \alpha_h}^T$, we have on the left hand side of the above as,

$$M_h^{-T}\frac{\partial f_h}{\partial \alpha_h}^T \left(R\, \frac{\partial n_1}{\partial \alpha_1} + \frac{\partial n_h}{\partial \alpha_h} M_h^{-1} R_\psi M_1\right)\dot{\alpha}_1. \tag{89}$$

Since

$$M_h^{-T}\frac{\partial f_h}{\partial \alpha_h}^T = \frac{\partial f_h}{\partial \alpha_h} M_h^{-1} = \left(R\, \frac{\partial f_1}{\partial \alpha_1} M_1^{-1} R_\psi\right)^T = R_\psi\, M_1^{-T} \frac{\partial f_1}{\partial \alpha_1}^T R^T, \tag{90}$$

equation (89) becomes

$$\dot{\alpha}_1 \left(R_\psi\, M_1^{-T} \frac{\partial f_1}{\partial \alpha_1}^T \frac{\partial n_1}{\partial \alpha_1} + M_h^{-T} \frac{\partial f_h}{\partial \alpha_h}^T \frac{\partial n_h}{\partial \alpha_h} M_h^{-1} R_\psi M_1\right) = \left(R_\psi\, M_1^{-T} \frac{\partial f_1}{\partial \alpha_1}^T \frac{\partial n_1}{\partial \alpha_1} M_1^{-1} R_\psi + M_h^{-T} \frac{\partial f_h}{\partial \alpha_h}^T \frac{\partial n_h}{\partial \alpha_h} M_h^{-1}\right) \times R_\psi M_1 \dot{\alpha}_1. \tag{91}$$

Setting

$$\tilde{\mathcal{K}}_1 = R_\psi\, M_1^{-T} \frac{\partial f_1}{\partial \alpha_1}^T \frac{\partial n_1}{\partial \alpha_1} M_1^{-1} R_\psi$$

and

$$\mathcal{K}_h = M_h^{-T} \frac{\partial f_h}{\partial \alpha_h}^T \frac{\partial n_h}{\partial \alpha_h} M_h^{-1},$$

it follows from (87) that

$$\left(\tilde{\mathcal{K}}_1 + \mathcal{K}_h\right) R_\psi M_1 \dot{\alpha}_1 = M_h^{-T} \frac{\partial f_h}{\partial \alpha_h}^T \left[-\dot{R}\, n_1 - \frac{\partial n_h}{\partial \alpha_h} M_h^{-2} \frac{\partial f_h}{\partial \alpha_h}^T \left(\dot{R}\, f_1 + \dot{p}\right)\right] = -M_h^{-T} \frac{\partial f_h}{\partial \alpha_h}^T \dot{R}\, n_1 - \mathcal{K}_h\, M_h^{-T} \frac{\partial f_h}{\partial \alpha_h}^T \left(\dot{R}\, f_1 + \dot{p}\right) \tag{92}$$

so that

$$\dot{\alpha}_1 = \left(\tilde{\mathcal{K}}_1 + \mathcal{K}_h\right)^{-1} R_\psi M_1^{-1} \times \left[\underbrace{-M_h^{-T} \frac{\partial f_h}{\partial \alpha_h}^T \dot{R}\, n_1}_{w_t} - \mathcal{K}_h \underbrace{M_h^{-T} \frac{\partial f_h}{\partial \alpha_h}^T \left(\dot{R}\, f_1 + \dot{p}\right)}_{v_t}\right] \tag{93}$$

or

$$\dot{\alpha}_1 = \left(\tilde{\mathcal{K}}_1 + \mathcal{K}_h\right)^{-1} R_\psi M_1^{-1}(w_t - \mathcal{K}_h v_t). \tag{94}$$

Finding the generalized velocity of the head with respect to a single IAB deformation is tantamount to finding $(\hat{w}, v) = \dot{g}\, g^{-1}$. Thus,

$$\omega_t = -M_h^{-T} \frac{\partial f_h}{\partial \alpha_h}^T (\omega \times (R\, n_1)) = -M_h^{-T} \frac{\partial f_h}{\partial \alpha_h}^T (n_h \times \omega) \tag{95}$$

$$v_t = M_h^{-T} \frac{\partial f_h}{\partial \alpha_h}^T (\omega \times (R\, f_1) + \omega \times p + v) \tag{96}$$

$$= M_h^{-T} \frac{\partial f_h}{\partial \alpha_h}^T (-f_h \times \omega + v), \tag{97}$$

where ω_t is the head's rolling velocity projected onto the contact's tangent plane. The rotation normal to the surface is canceled by the cross product of ω and n_h. In the same vein, v_t is the sliding velocity between the contacts, projected onto the tangent plane. Following the above construction, we find the kinematics of the contact point of the head in local coordinates is

$$\dot{\alpha}_h = M_h^{-1} \left(\tilde{\mathcal{K}}_1 + \mathcal{K}_h\right)^{-1} (\omega_t - \tilde{\mathcal{K}}_1 v_t), \tag{98}$$

where $\left(\tilde{\mathcal{K}}_1 + \mathcal{K}_h\right)$ is the *relative curvature* [31]. It remains to solve for the relative orientation between the two local coordinates, ψ.

B. Relative Contact Orientation and Torsion Metric Tensors

In matrix form, (84b) and (84c) can be written as,

$$R\begin{bmatrix}\frac{\partial f_1}{\partial \alpha_1}M_1^{-1} & n_1(\alpha_1)\end{bmatrix}\begin{bmatrix}R_\psi & 0\\ 0 & -1\end{bmatrix}=\begin{bmatrix}\frac{\partial f_h}{\partial \alpha_h}M_h^{-1} & n_h(\alpha_h)\end{bmatrix}. \tag{99}$$

Following the normalized Gaussian frame defined in (30), we can rewrite the above equation as

$$R[x_1\, y_1\, z_1]\bar{R}_\psi = [x_h\, y_h\, z_h]. \tag{100}$$

The total derivative of (100) yields

$$\dot{R}\begin{bmatrix}x_1 & y_1 & z_1\end{bmatrix}\bar{R}_\psi + R\begin{bmatrix}\dot{x}_1 & \dot{y}_1 & \dot{z}_1\end{bmatrix}\bar{R}_\psi + R\begin{bmatrix}x_1 & y_1 & z_1\end{bmatrix}\begin{bmatrix}\dot{R}_\psi & 0\\ 0 & 0\end{bmatrix} = \begin{bmatrix}\dot{x}_h\\ \dot{y}_h\\ \dot{z}_h\end{bmatrix}^T. \tag{101}$$

Premultiplying by $y_1^T R^T$ and then postmultiplying by $\bar{R}_\psi\begin{pmatrix}1\\0\\0\end{pmatrix}$, with the knowledge that $\bar{R}_\psi\bar{R}_\psi = \mathbf{I}$, and the identity $y_1^T y_1 = 1$, we find that

$$y_1^T R^T\dot{R}[x_1\ y_1\ z_1]\bar{R}_\psi + y_1^T[\dot{x}_1,\ \dot{y}_1,\ \dot{z}_1]\bar{R}_\psi + (0\ 1\ 0)\begin{bmatrix}\dot{R}_\psi & 0\\ 0 & 0\end{bmatrix} = y_1^T R^T[\dot{x}_h\ \dot{y}_h\ \dot{z}_h] \tag{102}$$

$$y_1^T R^T\dot{R}x_1 + y_1^T\dot{x}_1 + (0\ 1\ 0)\begin{bmatrix}\dot{R}_\psi R_\psi & 0\\ 0 & 0\end{bmatrix}\begin{pmatrix}1\\0\\0\end{pmatrix} = y_1^T R^T[\dot{x}_h\ \dot{y}_h\ \dot{z}_h]\bar{R}_\psi\begin{pmatrix}1\\0\\0\end{pmatrix} \tag{103}$$

$$y_1^T R^T\dot{R}x_1 + y_1^T\dot{x}_1 + (0\quad 1)\begin{bmatrix}0 & \dot{\psi}\\ -\dot{\psi} & 0\end{bmatrix}\begin{pmatrix}1\\0\end{pmatrix} = y_1^T R^T[\dot{x}_h\ \dot{y}_h\ \dot{z}_h]\bar{R}_\psi\begin{pmatrix}1\\0\\0\end{pmatrix} \tag{104}$$

$$y_1^T R^T\dot{R}x_1 + y_1^T\dot{x}_1 - \dot{\psi} = y_1^T R^T[\dot{x}_h\ \dot{y}_h\ \dot{z}_h]\bar{R}_\psi\begin{pmatrix}1\\0\\0\end{pmatrix}. \tag{105}$$

From (100), we have that

$$\bar{R}_\psi^T\begin{bmatrix}x_1^T & y_1^T & z_1^T\end{bmatrix}R^T = \begin{bmatrix}x_h^T & y_h^T & z_h^T\end{bmatrix} \tag{106}$$

so that

$$\begin{bmatrix}x_1^T & y_1^T & z_1^T\end{bmatrix}R^T = \bar{R}_\psi\begin{bmatrix}x_h^T & y_h^T & z_h^T\end{bmatrix} \tag{107}$$

or

$$y_1^T R^T = (0\ 1\ 0)\,\bar{R}_\psi\begin{bmatrix}x_h^T & y_h^T & z_h^T\end{bmatrix} = (0\ 1)\,R_\psi\begin{pmatrix}x_h^T\\ y_h^T\end{pmatrix}. \tag{108}$$

It follows from (105) that

$$\dot{\psi} = y_1^T R^T\dot{R}x_1 + y_1^T\frac{\partial x_1}{\partial \alpha_1}\dot{\alpha}_1 - (0,\,1)\,R_\psi\begin{bmatrix}x_h^T\dot{x}_h & x_h^T\dot{y}_h\\ y_h^T\dot{x}_h & y_h^T\dot{y}_h\end{bmatrix}R_\psi\begin{pmatrix}1\\0\end{pmatrix}. \tag{109}$$

Using the identities,

$$x_i^T y_i = 0,\implies \dot{x}_i^T y_i = -x_i^T\dot{y}_i = y_i^T\dot{x}_i \tag{110}$$

$$x_i^T x_i = 1,\implies \dot{x}_i^T x_i = 0, \tag{111}$$

we can rewrite (109) as

$$\dot{\psi} = y_1^T\,R^T\dot{R}\,x_1 + y_h^T\frac{\partial x_h}{\partial \alpha_h}\,\dot{\alpha}_h + y_1^T\frac{\partial x_1}{\partial \alpha_1}\,\dot{\alpha}_1 = \omega_n + T_h\,M_h\,\dot{\alpha}_h + T_1\,M_1\dot{\alpha}_1 \tag{112}$$

where

$$\omega_n = y_1^T\,R^T\,\dot{R}x_1 = (R\,y_1)^T\,w\times(Rx_1) = (R\,z_1)^T\,\omega = z_h^T\,\omega \tag{113}$$

$$T_h = y_h\frac{\partial x_h^T}{\partial \alpha_h}M_h^{-T},\qquad T_1 = y_1\frac{\partial x_1^T}{\partial \alpha_1}M_1^{-T}. \tag{114}$$

It follows that the first, second and third equations of contact are given by (94), (98), and (112) respectively, *i.e.*

Equations of Contact

$$\dot{\alpha}_1 = \left(\tilde{\mathcal{K}}_1 + \mathcal{K}_h\right)^{-1}R_\psi M_1^{-1}(\omega_t - \mathcal{K}_h v_t) \tag{115a}$$

$$\dot{\alpha}_h = M_h^{-1}\left(\tilde{\mathcal{K}}_1 + \mathcal{K}_h\right)^{-1}(\omega_t - \tilde{\mathcal{K}}_1 v_t) \tag{115b}$$

$$\dot{\psi} = \omega_n + T_h\,M_h\,\dot{\alpha}_h + T_1\,M_1\dot{\alpha}_1. \tag{115c}$$

Appendix C
Base IAB-Head Boundary Value Problem

In general, we expect that the side IAB chains will preserve spherically symmetric deformation since the side force from the object is minimal. Again, the spherical deformation principle is a first order approximation to aid a simplified model. For the base IABs in the closed kinematic chain, it is natural to expect the the IABs will exhibit inhomogeneous deformation. For non-isochoric deformations, finding a closed-form kinematic solution for the deformation will be difficult without other restrictions on the nature of the deformation. Suppose the deformation along the radial axis is inextensible, then the deformation of the spherical shell is characterized by $\boldsymbol{x} = f(R)\boldsymbol{X}$, where $R = |\boldsymbol{X}|$ and $f(R) = 1 + \frac{r_i - R_i}{R}$. It can be verified that the change in total volume is

$$\Delta V = 4\pi(R_\circ - R_i)(r_i r_\circ - R_i R_\circ). \tag{116}$$

In this appendix, we derive the kinematics that governs such deformations. The kinematics for the side IAB chains holds

from equations 24-27 of [1]. When the IAB dents, we rewrite the deformation gradient as

$$\mathbf{F} = \begin{bmatrix} \frac{R^2}{r^2} & 0 & 0 \\ 0 & \frac{r}{R} & f(R) \\ 0 & 0 & \frac{r}{R} \end{bmatrix} = \begin{bmatrix} \frac{R^2}{r^2} & 0 & 0 \\ 0 & \frac{r}{R} & 1 + \frac{r_i - R_i}{R} \\ 0 & 0 & \frac{r}{R} \end{bmatrix}. \quad (117)$$

Given the incompressibility properties of the IAB material wall (made out of elastomers such as natural/synthetic rubber, polyurethane etc) – materials that exhibit a Poisson ratio of ideally 0.5 [32], we can determine the contribution of internal pressure on the deformation by making the assumption that on an arbitrarily chosen subsection of the IAB material, the components of the stress matrix satisfy hydrostatic equilibrium so that the effect of the stress cancels out on the elastic properties of the material([14], [37]).

Recall the equation of equilibrium in spherical coordinates,

$$-b_r = \frac{1}{r^2}\frac{\partial r^2 \sigma_{rr}}{\partial r} + \frac{1}{r\sin\phi}\frac{\partial \sin\phi \sigma_{r\phi}}{\partial \phi} + \frac{1}{r\sin\phi}\frac{\partial \sigma_{r\theta}}{\partial \theta} - \frac{1}{r}(\sigma_{\theta\theta} + \sigma_{\phi\phi}) \quad (118a)$$

$$-b_\phi = \frac{1}{r^3}\frac{\partial r^3 \sigma_{r\phi}}{\partial r} + \frac{1}{r\sin\phi}\frac{\partial \sin\phi \sigma_{\phi\phi}}{\partial \phi} + \frac{1}{r\sin\phi}\frac{\partial \sigma_{\theta\phi}}{\partial \theta} - \frac{\cot\phi}{r}(\sigma_{\theta\theta}) \quad (118b)$$

$$-b_\theta = \frac{1}{r^3}\frac{\partial r^3 \sigma_{\theta r}}{\partial r} + \frac{1}{r\sin^2\phi}\frac{\partial \sin^2\phi \sigma_{\theta\phi}}{\partial \phi} + \frac{1}{r\sin\phi}\frac{\partial \sigma_{\theta\theta}}{\partial \theta} \quad (118c)$$

The assumed regularity of the IAB in the reference configuration leads to the steady state conditions for Cauchys first equation so that the stress tensor field $\boldsymbol{\sigma}$ becomes self-equilibrated by virtue of its spatial divergence and its symmetric properties *i.e.*

$$\mathbf{div}\ \boldsymbol{\sigma} = 0. \quad (119)$$

Equation (119) is only valid if the hydrostatic pressure p in equation (15) of [1] is independent of θ and ϕ so that the components, $\sigma_{r\phi}, \sigma_{r\theta}$ in the equilibrium equations for the body force vanish and we are left with

$$\frac{1}{r^2}\frac{\partial}{\partial r}(r^2\sigma_{rr}) = (\sigma_{\theta\theta} + \sigma_{\phi\phi}). \quad (120a)$$

$$\frac{\partial}{\partial \phi}(\sigma_{\phi\phi}\ \sin\phi) = \cos\phi(\sigma_{\theta\theta}). \quad (120b)$$

$$\frac{1}{r\sin\phi}\frac{\partial}{\partial \theta}(\sigma_{\theta\theta}) = 0. \quad (120c)$$

In general, we are interested in hydrostatic equilibrium equation (120a) owing to the nature of the deformation. Again, we integrate (120a) as in [1] but with the values of the stress components compensated for in the shear term, $1 + \frac{r_i - R_i}{R}$.

D Acknowledgment

The author would like to thank Erik Pearson for kindly providing the CAD models of the couch and gantry used in our SOFA simulation. A vote of thanks to Ariella Mansfield for pointing out faculty with relevant expertise at Penn Engineering. In particular, thanks to Professor James Pikul at Penn Mechanical Engineering for insightful discussions.

References

[1] O. Ogunmolu, X. Liu, and R. Wiersma, "Mechanism and Constitutive Model of a Continuum Robot for Head and Neck Cancer Radiotherapy," 2019. 1, 4, 5, 6, 7, 9, 11, 14

[2] O. P. Ogunmolu, "A Multi-DOF Soft Robot Mechanism for Patient Motion Correction and Beam Orientation Selection in Cancer Radiation Therapy." Ph.D. dissertation, The University of Texas at Dallas; UT Southwestern Medical Center, 2019. 1, 2, 4

[3] J. M. Bern, K.-H. Chang, and S. Coros, "Interactive design of animated plushies," *ACM Transactions on Graphics (TOG)*, vol. 36, no. 4, p. 80, 2017. 1

[4] J. M. Bern, G. Kumagai, and S. Coros, "Fabrication, modeling, and control of plush robots," in *2017 IEEE/RSJ International Conference on Intelligent Robots and Systems (IROS)*. IEEE, 2017, pp. 3739–3746. 1

[5] T. Liu, S. Bouaziz, and L. Kavan, "Quasi-newton methods for real-time simulation of hyperelastic materials," *ACM Transactions on Graphics (TOG)*, vol. 36, no. 3, p. 23, 2017. 1

[6] S. Bouaziz, S. Martin, T. Liu, L. Kavan, and M. Pauly, "Projective dynamics: fusing constraint projections for fast simulation," *ACM Transactions on Graphics (TOG)*, vol. 33, no. 4, p. 154, 2014. 1

[7] U.S. Department of Health and Human Services, National Institutes of Health, National Cancer Institute. (2019) Cancer Stat Facts: Cancer of Any Site. [Online]. Available: https://seer.cancer.gov/statfacts/html/all.html 1

[8] M. D. Michaelson, S. E. Cotter, P. C. Gargollo, A. L. Zietman, D. M. Dahl, and M. R. Smith, "Management of complications of prostate cancer treatment," *CA: a cancer journal for clinicians*, vol. 58, no. 4, pp. 196–213, 2008. 1

[9] M. Giorelli, F. Renda, M. Calisti, A. Arienti, G. Ferri, and C. Laschi, "Neural Network And Jacobian Method For Solving The Inverse Statics Of A Cable-driven Soft Arm With Nonconstant Curvature," *IEEE Transactions on Robotics*, vol. 31, no. 4, pp. 823–834, 2015. 1

[10] O. Ogunmolu, A. Kulkarni, Y. Tadesse, X. Gu, S. Jiang, and N. Gans, "Soft-neuroadapt: A 3-dof neuro-adaptive patient pose correction system for frameless and maskless cancer radiotherapy," in *IEEE/RSJ International Conference on Intelligent Robots and Systems (IROS), Vancouver, BC, CA*. IEEE, 2017, pp. 3661–3668. 1, 2, 3

[11] H. Mochiyama, "Hyper-flexible robotic manipulators," in *IEEE International Symposium on Micro-NanoMechatronics and Human Science, 2005*. IEEE, 2005, pp. 41–46. 1

[12] G. S. Chirikjian and J. W. Burdick, "The kinematics of hyper-redundant robot locomotion," *IEEE transactions on robotics and automation*, vol. 11, no. 6, pp. 781–793, 1995. 1

[13] F. Renda and L. Seneviratne, "A Geometric and Unified Approach for Modeling Soft-Rigid Multi-body Systems with Lumped and Distributed Degrees of Freedom," *2018 IEEE International Conference on Robotics and Automation (ICRA)*, pp. 1567 – 1574, 2018. 1

[14] H. Demirkoparan and T. J. Pence, "Swelling of an Internally Pressurized Nonlinearly Elastic Tube with Fiber Reinforcing," *International journal of solids and structures*, vol. 44, no. 11-12, pp. 4009–4029, 2007. 1, 14

[15] A. Sedal, D. Bruder, J. Bishop-Moser, R. Vasudevan, and S. Kota, "A continuum model for fiber-reinforced soft robot actuators," *Journal of Mechanisms and Robotics*, vol. 10, no. 2, p. 024501, 2018. 1

[16] T. George Thuruthel, Y. Ansari, E. Falotico, and C. Laschi, "Control Strategies for Soft Robotic Manipulators: A Survey," *Soft Robotics*, vol. 5, no. 2, pp. 149–163, 2018. 2, 3

[17] O. Ogunmolu, N. Gans, S. Jiang, and X. Gu, "An Image Guided Soft Robotic Patient Positioning System for Maskless Head And Neck Cancer Radiotherapy: A Proof of Concept Study," *Medical Physics: The International Journal of Medical Physics Research and Practice*, vol. 42, pp. 3266–3266, June 2015. 2

[18] O. P. Ogunmolu, X. Gu, S. Jiang, and N. R. Gans, "A real-time, soft robotic patient positioning system for maskless head-and-neck cancer radiotherapy: An initial investigation," in *Automation Science and Engineering (CASE), 2015 IEEE International Conference on, Gothenburg, Sweden*. IEEE, 2015, pp. 1539–1545. 2

[19] O. P. Ogunmolu, X. Gu, S. Jiang, and N. R. Gans, "Vision-based control of a soft robot for maskless head and neck cancer radiotherapy," in *Automation Science and Engineering (CASE), 2016 IEEE International Conference on, Fort Worth, Texas*. IEEE, 2016, pp. 180–187. 2

[20] O. Ogunmolu and R. D. Wiersma, *Towards Real-Time Motion Compensation in Radio-Transparent Robotic Radiation Therapy.* 2

[21] M. Mooney, "A theory of large elastic deformation," *Journal of applied physics*, vol. 11, no. 9, pp. 582–592, 1940. 3, 6

[22] R. Ogden, *Non-linear Elastic Deformations*. Mineola, New York: Dover Publicationbs, Inc., 1997. 3, 4, 6, 9

[23] L. R. G. Treloar, *The physics of rubber elasticity*. Oxford University Press, USA, 1975. 3

[24] M. W. Hannan and I. D. Walker, "Kinematics and the Implementation of an Elephant's Trunk Manipulator and Other Continuum Style Robots," *Journal of Robotic Systems*, vol. 20, no. 2, pp. 45–63, 2003. 3

[25] M. W. Hannan and I. D. Walker, "Novel Kinematics for Continuum Robots." Advances in Robot Kinematics, 2000, pp. 227–238. 3

[26] B. A. Jones and I. D. Walker, "Kinematics for Multisection Continuum Robots.pdf," vol. 22, no. 1, pp. 43–55, 2006. 3

[27] A. D. Kapadia, K. E. Fry, and I. D. Walker, "Empirical investigation of closed-loop control of extensible continuum manipulators," in *2014 IEEE/RSJ International Conference on Intelligent Robots and Systems*. IEEE, 2014, pp. 329–335. 3

[28] F. Renda, M. Giorelli, M. Calisti, M. Cianchetti, and C. Laschi, "Dynamic model of a multibending soft robot arm driven by cables," *IEEE Transactions on Robotics*, vol. 30, no. 5, pp. 1109–1122, 2014. 3

[29] D. Trivedi, A. Lotfi, and C. D. Rahn, "Geometrically Exact Models For Soft Robotic Manipulators," *IEEE Transactions on Robotics*, vol. 24, no. 4, pp. 773–780, 2008. 3

[30] V.-D. Nguyen, "Constructing force-closure grasps," *The International Journal of Robotics Research*, vol. 7, no. 3, pp. 3–16, 1988. 5

[31] D. J. Montana, "The Kinematics of Contact And Grasp," *The International Journal of Robotics Research*, vol. 7, no. 3, pp. 17–32, 1988. 5, 8, 12

[32] A. Gent, *Engineering with Rubber. How to Design Rubber Components*. Munich: Carl Hanser Verlag Publicationbs, 2012. 6, 14

[33] M. Spivak, "A Comprehensive Introduction to Differential Geometry. Vol. V. Berkeley: Publish or Perish," *Inc. XI*, 1979. 7

[34] R. M. Murray and S. Sastry, "Grasping and Manipulation using Multifingered Robot Hands." in *Proceedings of Symposia in Applied Mathematics*, vol. 41, 1990, pp. 329–335. 7, 12

[35] C. Truesdell and W. Noll, *The Non-Linear Field Theories of Mechanics*. Springer, 1965. 8

[36] J. R. Kerr, "An Analysis of Multi-Fingered Hands," *International Journal of Robotics Research*, no. Dept. of Mechanical Engineering, pp. 3–17, 1984. 10

[37] G. A. Holzapfel, T. C. Gasser, and R. W. Ogden, "A new constitutive framework for arterial wall mechanics and a comparative study of material models," *Journal of elasticity and the physical science of solids*, vol. 61, no. 1-3, pp. 1–48, 2000. 14